THE UNIVERSITY *of* EDINBURGH

Edinburgh Research Explorer

The apical protein Apnoia interacts with Crumbs to regulate tracheal growth and inflation

The apical protein Apnoia interacts with Crumbs to regulate tracheal growth and inflation
--Manuscript Draft--

Manuscript Number:	PGENETICS-D-18-01254R1
Full Title:	The apical protein Apnoia interacts with Crumbs to regulate tracheal growth and inflation
Short Title:	Apnoia interacts with Crumbs to regulate tracheal growth and inflation
Article Type:	Research Article
Section/Category:	General
Keywords:	airway tube; retromer; Drosophila; larva
Corresponding Author:	Elisabeth Knust Max-Planck Institute Dresden, GERMANY
Corresponding Author's Institution:	Max-Planck Institute
First Author:	Kassiani Skouloudaki
Order of Authors:	Kassiani Skouloudaki
	Dimitrios K. Papadopoulos
	Pavel Tomancak
	Elisabeth Knust
Abstract:	Most organs of multicellular organisms are built from epithelial tubes. To exert their functions, tubes rely on apico-basal polarity, on junctions, which form a barrier to separate the inside from the outside, and on a proper lumen, required for gas or liquid transport. Here we identify apnoia (apn), a novel Drosophila gene required for tracheal tube elongation and lumen stability at larval stages. Larvae lacking Apn show abnormal tracheal inflation and twisted airway tubes, but no obvious defects in early steps of tracheal maturation. apn encodes a transmembrane protein, primarily expressed in the tracheae, which exerts its function by controlling the localization of Crumbs (Crb), an evolutionarily conserved apical determinant. Apn physically interacts with Crb to control its localization and maintenance at the apical membrane of developing airways. In apn mutant tracheal cells, Crb fails to localize apically and is trapped in retromer-positive vesicles. Consistent with the role of Crb in apical membrane growth, RNAi-mediated knockdown of Crb results in decreased apical surface growth of tracheal cells and impaired axial elongation of the dorsal trunk. We conclude that Apn is a novel regulator of tracheal tube expansion in larval tracheae, the function of which is mediated by Crb.
Suggested Reviewers:	Claire Thomas Pennsylvania State University University Park : Penn State clairet@psu.edu Cell polarity, adhesion and morphogenesis in Drosophila development
	Antoine Guichet Institut Jacques Monod antoine.guichet@igm.fr Polarity and morphogenesis in Drosophila development
	Anne Uv Goteborgs Universitet anne.uv@medkem.gu.se Epithelial tubes
	Stefan Luschnig Westfalische Wilhelms-Universitat Munster luschnig@uni-muenster.de Epithelial tubes

Opposed Reviewers:	Shigeo Hayashi Riken Center for Developmental Biology Conflict of interest, works on cloesely related topics
	Ulrich Tepass University of Toronto Conflict of interest, works on cloesely related topics
	Marta Llimargas Institut of Molecular Biology Barcelona Conflict of interest, works on cloesely related topics
	Christos Samakovlis Stockholms Universitet Published with the first author while she was a postdoc with him.

Additional Information:	
Question	**Response**
Financial Disclosure Enter a financial disclosure statement that describes the sources of funding for the work included in this submission. Review the submission guidelines for detailed requirements. View published research articles from *PLOS Genetics* for specific examples. This statement is required for submission and **will appear in the published article** if the submission is accepted. Please make sure it is accurate.	The research was supported by the Max-Planck Society. The funders had no role in study design, data collection and analysis, decision to publish, or preparation of the manuscript.

* typeset

Competing Interests

Use the instructions below to enter a competing interest statement for this submission. On behalf of all authors, disclose any competing interests that could be perceived to bias this work—acknowledging all financial support and any other relevant financial or non-financial competing interests.

This statement **will appear in the published article** if the submission is accepted. Please make sure it is accurate. View published research articles from *PLOS Genetics* for specific examples.

The authors have declared that no competing interests exist.

* typeset

Data Availability

Authors are required to make all data underlying the findings described fully available, without restriction, and from the time of publication. PLOS allows rare exceptions to address legal and ethical concerns. See the PLOS Data Policy and FAQ for detailed information.

A Data Availability Statement describing where the data can be found is required at submission. Your answers to this question constitute the Data Availability Statement and will be published in the article, if accepted.

Do the authors confirm that all data underlying the findings described in their manuscript are fully available without restriction?

Yes - all data are fully available without restriction

Describe where the data may be found in full sentences. If you are copying our sample text, replace any instances of XXX with the appropriate details. • If the data are **held or will be held in a public repository**, include URLs, accession numbers or DOIs. If this information will only be available after acceptance, indicate this by ticking the box below. For example: *All XXX files are available from the XXX database (accession number(s) XXX, XXX.).* • If the data are all contained **within the manuscript and/or Supporting Information files**, enter the following: *All relevant data are within the manuscript and its Supporting Information files.* • If neither of these applies but you are able to provide **details of access elsewhere**, with or without limitations, please do so. For example: *Data cannot be shared publicly because of [XXX]. Data are available from the XXX Institutional Data Access / Ethics Committee (contact via XXX) for researchers who meet the criteria for access to confidential data.* *The data underlying the results presented in the study are available from (include the name of the third party and contact information or URL).* • This text is appropriate if the data are owned by a third party and authors do not have permission to share the data. * typeset	All relevant data are within the paper and its Supporting Information files
Additional data availability information:	Tick here if the URLs/accession numbers/DOIs will be available only after acceptance of the manuscript for publication so that we can ensure their inclusion before publication.

CBG
Max Planck Institute
of Molecular Cell Biology
and Genetics
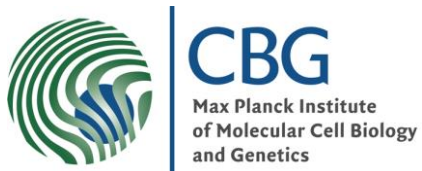
PFOTENHAUERSTR. 108
01307 DRESDEN
Tel.: (0351) 210-1300
FAX: (0351) 210-1309
e-mail: knust@mpi-cbg.de

PROF. DR. ELISABETH KNUST

Dresden, 31.10.2018

Dear Editor,

we would like to submit the revised version of our manuscript entitled **"The apical protein Apnoia interacts with Crumbs to regulate tracheal growth and inflation"** for publication in PLoS Genetics.

We have addressed all points raised by the reviewers and listed them in a separate file.

We hope that you find our work interesting and are looking forward to your response.

Sincerely,

Elisabeth Knust
Kassiani Skouloudaki

Responses to reviewer's questions

Reviewer #1:

In their manuscript entitled "The apical protein Apnoia interacts with Crumbs to regulate tracheal growth and inflation," Skouloudaki, Papadopoulos and colleagues identify a novel Crumbs-interacting protein, Apnoia (Apn), which they name based on the tracheal defect observed in loss of function animals. Apn was initially identified by yeast two-hybrid as a Crumbs interactor and later shown to substantially co-localize with Crumbs in tracheal cells, although most Apn is apical as compared tot he subapical localization of Crb. A CRISPR-Cas9 generated deletion of the coding region resulted in a lethal mutation in which animals die during the second larval instar with twisted and uninflated tracheal tubes. Tube maturation was assessed and found to be defective at the stage of liquid clearance and gas-filling. Additionally, authors report that dorsal trunk tubes displayed a reduced length. Based on measurements of cells within the dorsal trunk, the authors conclude that growth along the AP axis is reduced, but not circumferential growth. In addition, the authors report that Crumbs localization is altered such that Crb is mostly within intracellular vesicles. Blocking endocytosis in an apn mutant background resulted in apical accumulation of Crbs, interrupted by the authors as indicating a requirement for Apn in Crb retention at the apical membrane, perhaps via Rab11-dependent trafficking from an endosomal compartment. The intracellular Crb in apn mutant animals was largely colocalized with the retromer component, VPS-35. The authors further report that knockdown of Crb by RNAi recapitulates the apn loss of function phenotype.

The work is interesting and appropriate for the journal. It seems largely well done, and should be considered for publication after addressing the following concerns:

• A major deficit of this manuscript is that the authors test a tracheal requirement for Crumbs and Apn by eliminating protein function in the entire animal. Crumbs, of course, is broadly expressed, and while apn expression does seem to be fairly tracheal-specific, there remains a worry that the phenotype is non-autonomous. In principle these deficits could be easily addressed.

> Since *apn* is expressed only in tracheae, its elimination in the entire animal is expected to influence only the tracheal tissue. In addition, tracheae-specific depletion of apn by RNAi exhibits the same phenotype (Suppl. Fig 3B). Finally, re-introduction of the apn cDNA in the tracheae rescues the mutant phenotype (Suppl. Fig 3C, F).

Complicating matters for Crumbs, mosaic loss of function studies in the trachea have been performed (crb11A22), and no defect reported (Schottenfeld-Roames et al., 2014). Likewise, pan-tracheal crumbs RNAi has been shown to modify the phenotype of mutants that accumulate ectopically high levels of Crumbs, but has not been shown to cause tracheal tube defects in otherwise wild type backgrounds (Song et al., 2013), at least under the RNAi conditions described. Authors should test cell autonomy or at least tracheal-specific requirements for Crb and Apn, either by eliminating them there specifically, and/or by rescuing specifically in the trachea (in the case of apn mutant larvae).

> We thank the reviewer for this important question. We have actually used different reagents from Song et al, 2013, indicated in Materials and Methods, in which we describe the crb RNAi line used by us. Indeed, previous data performed with crb[11A22] as well as with crb RNAi #

39177 did not show significant tracheal defects. In line with this, crb[11A22] and crbRNAi 39177 showed no abnormal trachea phenotype in our experiments (data not shown). Therefore we tested the crb RNAi #38373 (Hochapfel F et al., 2017, Cellular and Molecular Life Sciences), which targets the 3'UTR of the crb mRNA. We observed a trachea-specific phenotype upon knocked down, using either ubiquitously of tracheal-specific Gal4 drivers.

The same phenotypes were observed upon Apn knock-down using the aforementioned drivers. Personal communication with Michael Krahn (University of Muenster) confirmed that these authors also experienced problems with the Song et al *crb* RNAi line #39177, but not with the *crb* RNAi line #38373. Therefore we decided to perform our knockdown experiments with the line #38373 line provided by the Bloomington Stock Center.

Additional points for the authors to address include:

• Can apn mutants be rescued with transgene expression during larval stages?

New data added in Suppl. Fig 3C, F show that in approximately 20% of *apn¹* mutant larvae gas filling (Suppl. Fig 3C) and tube length defects (Suppl. Fig 3F) are rescued upon tracheal-specific transgene expression.

• Is Crb localization in other epithelia normal in apn mutants?

New data added in Suppl. Fig 4G, H, show that Crb localization is not altered in salivary glands of stage L2 mutant in *apn¹* larvae.

• Are tracheal defects, including Crb mislocalization, limited to multicellular tracheal tubes? or are autocellular and seamless tubes also compromised?

New data added in (Suppl. Fig 4A-B''') show that tracheal defects are not limited to multicellular tubes, but also affect autocellular and seamless tubes.

For the PLA shown in figure 1, can authors show images from more closely matched dorsal trunk segments (same metamere and same tube diameter) and provide quantitation?

We provide new data according to reviewer request in Fig. 2A-B" and Fig. 2C.

Reviewer #2:
Through a modified yeast two hybrid screen, Skouloudaki et al identify an insect-specific transmembrane protein, which they name Apnoia (Apn), as an interaction partner of the apical determinant Crumbs. Further evidence for a complex comes from co-IPs from

cultured cells and from in vivo localization data. Apn is shown to have high expression in the Drosophila tracheal system, localizing to the apical domain of tracheal cells. Generated Apn mutants display tracheal defects specifically at larval stages when tracheal remodeling events are associated with larval molting and growth. The tracheal tubes of apn mutants are abnormally short and twisted, defects associated with abnormal apical domain size and shape. These defects are also associated with a loss of Crumbs from the apical domain and abnormal accumulation of Crb in Vps35-positive vesicles. Blocking endocytosis reverses the loss of cortical Crumbs in apn mutants, and the loss of Crumbs seems to underlie the apn mutant defects since similar defects are observed following crb RNAi. This study should be of interest to cell and developmental biologists, particularly those studying insects. However, a number of points should be addressed.

1. For Figure 1H, I and J, higher magnification X-Y images of the apical surface and circumference should be shown to clarify co-localization patterns. Also, is there any degree of Apn-Crb co-localization over the apical surface to corroborate the PLA data?

> In Fig.1G-G" and H-H"(X-Y) as well as Fig.1G"' and H"' (circumference Y-Z) we provide higher magnification images that clearly show a high degree of colocalization of Apn with the other apical membrane proteins.
> In Fig.1I-I" (X-Y) and Fig.1I"' (circumference Y-Z) we provide strong evidence that Crb and Apn partially colocalize at the apical cell surface.

2. Further controls are needed for the PLA experiments. The same antibodies should be used in the experiment and control (e.g. anti-Crb plus anti-GFP or anti-Apn plus anti-GFP).

> We apologize for not making this point clear in our manuscript. We have used a *D*ECad-GFP knock-in line as well as a fosmid expressing a GFP-tagged Apn. We stained both lines with GFP and Crb antibodies. This means that the same antibodies have been used in experiment (apn-sfGFP) and control (*D*Ecad-GFP).
> We have included an additional experiment in Fig.2D-D" and Fig.2E-E", in which the same line (apn-sfGFP) was used for PLA, but different antibodies (e.g. anti-Crb plus anti-GFP (Fig.2D-D") and anti-Ecad plus anti-GFP, as control (Fig.2E-E")).

A different apical protein should be tested for a PLA signal with Crb (a different GFP-tagged protein for example) since the signal between Crb and Apn-GFP could be due to random interactions in the apical domain rather than being due to specific complexes.

> We followed the reviewer's request and we used the apical protein SAS (SAS-Venus: Stranded-at-Second fused with Venus under the tubulin promoter). We stained both lines with anti-GFP and anti-Crb. This means that the same antibodies have been used in experiment (apn-sfGFP) (Fig.2F-F") and control (SAS-Venus) (Fig.2G-G").

3. To assess whether or not Apn has Crb-independent effects on retromer function, as considered in the Discussion, or if Apn affects the trafficking of other proteins through the retromer, it would be worth testing if the Vps35 compartment enlargement in apn mutants is due to Crb or not (by examining apn mutants expressing crb RNAi).

We thank the reviewer for his/her comment that allows us to clarify this point. We have performed additional experiments, in which *crb* was down regulated by RNAi in *apn¹* mutants. The results show that indeed the increase in size of Vps35 positive vesicles is to some extent dependent on Crb (new Fig. 10 A-D).

4. The authors say that the apn mutant phenotypes are also seen "in larvae upon knock-down of apn by RNAi in the tracheae (Fig. 2C)". However, the label for Fig 2C indicates that the apn RNAi is driven by the ubiquitous daughterless-Gal4. RNAi of apn specifically in the tracheal system is important for demonstrating that the tracheal defects are tissue-autonomous, and that the body size and viability defects are due the tracheal defects (also the body size and viability defects should be clearly described for the tracheal RNAi of apn). An alternate approach would be to attempt rescue of the mutant phenotypes with expression of Apn specifically in the tracheal system.

Following to the reviewer's comment, we performed tracheae-specific depletion of *apn* by RNAi and observed the same gas filling and tube length defects (Suppl. Fig 3B), defects in Crb localization (Fig 5R) as well as body size reduction (Suppl. Fig 2K) as in *apn¹* mutant animals.

New data added in Suppl. Fig 3C, F show that in approximately 20% of *apn¹* mutant larvae gas filling (Suppl. Fig 3C) and tube length defects (Suppl. Fig 3F) are rescued upon tracheal-specific transgene expression.

5. Similarly, the authors say that they "knocked-down crb in tracheal tubes by expressing crb RNAi" but again the panels in Figure 8 indicate the use of da-Gal4. RNAi of crb specifically in the tracheal system is also important for the author's conclusions.

We performed tissue specific depletion of *crb* by RNAi, and observed gas filling and tube length defects (Fig 3G), similar as in *apn¹* mutant animals.

A typo on page 10, line 242: Suppl. Fig. S3 D-E' should be Suppl. Fig. S3 E-F.'

We have corrected the manuscript according to reviewer's request.

1 **The apical protein Apnoia interacts with Crumbs to**

2 **regulate tracheal growth and inflation**

3

4 **Kassiani Skouloudaki[1,*,#], Dimitrios K. Papadopoulos[1,2,#], Pavel**

5 **Tomancak[1] and Elisabeth Knust[1,*]**

6 [1]Max-Planck Institute for Molecular Cell Biology and Genetics, 01307

7 Dresden, Germany

8

9 *Correspondence: knust@mpi-cbg.de and skouloud@mpi-cbg.de

10 #Equal contribution

11

12 [2]present address: MRC Human Genetics Unit, MRC Institute of

13 Genetics and Molecular Medicine at University of Edinburgh, Edinburgh,

14 United Kingdom

15

16

17

18 Running title:
19 Apnoia interacts with Crumbs to regulate tracheal growth and inflation
20
21 Key Words:
22 airway tube, retromer, *Drosophila*, larva
23

30

Abstract

Most organs of multicellular organisms are built from epithelial tubes. To exert
their functions, tubes rely on apico-basal polarity, on junctions, which form a
barrier to separate the inside from the outside, and on a proper lumen,
required for gas or liquid transport. Here we identify *apnoia* (*apn*), a novel
Drosophila gene required for tracheal tube elongation and lumen stability at
larval stages. Larvae lacking Apn show abnormal tracheal inflation and
twisted airway tubes, but no obvious defects in early steps of tracheal
maturation. *apn* encodes a transmembrane protein, primarily expressed in the
tracheae, which exerts its function by controlling the localization of Crumbs
(Crb), an evolutionarily conserved apical determinant. Apn physically interacts
with Crb to control its localization and maintenance at the apical membrane of
developing airways. In *apn* mutant tracheal cells, Crb fails to localize apically
and is trapped in retromer-positive vesicles. Consistent with the role of Crb in
apical membrane growth, RNAi-mediated knockdown of Crb results in
decreased apical surface growth of tracheal cells and impaired axial
elongation of the dorsal trunk. We conclude that Apn is a novel regulator of
tracheal tube expansion in larval tracheae, the function of which is mediated
by Crb.

Author summary

Tubular organs, such as the fruitfly airways, comprise essential functional
pipes through which gas and liquid are transported. They consist of highly
polarized epithelial cells that form a barrier between air and the larval body.
However, during larval development, these tubes, though very rigid due to the

2

56 presence of cuticle, need to rapidly grow in size within short time-windows. To

57 control their growth, cells have to regulate the apical membrane surface of the

58 epithelial cells. In this work we have discovered a new gene called *apnoia*,

59 which is important for tracheal growth and inflation at larval stages. We

60 demonstrate that Apnoia is expressed in the apical membrane of tracheal

61 epithelia cells, where it is required for apical membrane expansion. This

62 function is mediated by regulating the proper localization and maintenance of

63 the well-known apical determinant Crumbs. Both Apnoia and Crumbs proteins

64 are required for expansion of the apical cell surface and, thereby, tube

65 elongation. Such a mechanism is required to support the complex

66 morphogenetic events that the tracheal system undergoes during

67 development.

68

69 **Introduction**

70 Animal organs consist of epithelial tissues, which form the boundaries

71 between internal and external environment [1-3]. During development,

72 epithelia are instrumental to shape the various organs. Many epithelial tissues

73 form tubular organs, such as the gut, the kidney or the pulmonary system. A

74 fundamental feature of epithelial tubes and sheets is to keep the balance

75 between the maintenance of structural integrity and tissue rigidity during

76 organ growth and morphogenesis. To understand how this balance is

77 achieved during rapid, temporally regulated developmental transitions from

78 juvenile to adult body shapes, several studies in various animal models have

79 focused on elucidating how cell proliferation, cell polarity, cell shape changes

80 and trafficking contribute to the formation of tubular lumen length and

81 diameter [4-7]. The correct coordination of these processes is crucial for

82 normal organ function. This is reflected in the fact that several human

83 diseases are linked to defects in epithelial tube formation and maintenance,

84 such as polycystic kidney disease or cystic fibrosis [8-11].

85 The developing tracheae of *Drosophila melanogaster,* a network of

86 branched epithelial tubes that ensure oxygen supply to the cells of the body,

87 has emerged as an ideal system to study cell fate determination and

88 morphogenesis of epithelial tubes. The available genetic tools as well as the

89 ease to image the tracheal system in the fly embryo has provided detailed

90 insights into the developmental processes required to form tubular structures

91 with defined functional lumens and have contributed to elucidate the interplay

92 between tissue growth, differentiation and cell polarity [12-15].

93 The stereotypically branched tracheal system of *Drosophila* is set up at

94 mid-embryogenesis. Once a continuous tubular network has formed, the tube

95 expands to warrant increased oxygen supply to all tissues during animal

96 growth. Tube expansion occurs by growth along the diameter and along the

97 anterior-posterior axis. Growth is accompanied by the formation of a transient

98 cable, comprised of a chitinous apical extracellular matrix (aECM), which fills

99 the lumen of the tube. The generation of this cable requires the secretion of

100 chitin and chitin-modifying enzymes. Mutations in genes affecting secretion or

101 organization of the chitin cable result in excessively elongated tracheal tubes

102 or tubes with irregular diameter (with constricted and swollen areas along the

103 tube length) [15-17]. Axial growth, on the other hand, depends on the proper

104 elongation of tracheal cells along the anterior- posterior axis. At later stages of

105   embryogenesis, the lumen becomes cleared and filled with air.

106   After hatching, the larvae undergo two molts, a process during which

107   animals rapidly shed and replace their exoskeleton with a new one, bigger in

108   size. For this, new chitinous aECM is secreted apically, thus surrounding the

109   old tube. Remodeling of this aECM permits tissue growth between larval

110   molts. The molting process is initiated by the separation of the old aECM from

111   the apical surface of the epithelial cells and the secretion of chitinases and

112   proteinases, which partially degrade the old cuticle. The remnants of the old

113   cuticle in each metamer are shed through the spiracular branches. This

114   process, called ecdysis, is followed immediately by clearance of the molting

115   fluid and air filling [18-20]. Interestingly, while the diameter of the dorsal trunk

116   only increases at each molt, tube length increases continuously throughout

117   larval life, particularly during intermolt periods [14]. Despite the importance of

118   tube expansion and elongation for larval development [18], the underlying

119   mechanisms that control tracheal growth at this stage remain poorly

120   understood.

121   A well-established regulator of apical domain size in developing

122   epithelia is Crumbs (Crb). Crb is a type I transmembrane protein, which acts

123   as an apical determinant of epithelial tissues [21]. It has a large extracellular

124   domain, a single transmembrane and a short cytoplasmic domain. Loss- and

125   gain-of-function experiments have shown that apical levels of Crb are

126   important for proper cell polarity, tissue integrity and growth. For instance,

127   absence of Crb in embryonic epithelia can result in loss of apical identity and

128   disruption of epithelial organization [22-24]. In contrast, overexpression of Crb

129   can trigger apical membrane expansion, which can lead to a disordered

130 epithelium, abnormal expansion of tracheal tubes and/or tissue overgrowth

131 [21,25-33]. These results underscore the importance of Crb levels for

132 epithelial development and homeostasis.

133   Several mechanisms have been uncovered that ensure proper levels of

134 apical Crb. These include: stabilization of Crb at the membrane, mediated

135 through interactions of its cytoplasmic domain with scaffolding proteins, e.g.

136 Stardust (Sdt) or by homophilic interactions between Crb extracellular

137 domains [26,34-36], regulation of Crb trafficking, including endocytosis by AP-

138 2, Rab5 or Avalanche, membrane delivery by Rab11, recycling by the

139 retromer and endocytic sorting by the ESCRT III component Shrub/Vps32

140 [29,33,37-41].

141   To gain further insight into the molecular mechanisms that regulate Crb

142 and its activity during epithelial growth, we set out to identify novel interacting

143 partners of Crb by using the yeast two-hybrid system. One of the candidates

144 identified, CG15887, encodes a transmembrane protein, which localizes to

145 the apical surface of tracheal tubes. We found that the CG15887 protein

146 physically interacts with Crb. Based on the phenotype of mutations in

147 CG15887, which is characterized by defects in tracheal growth and inflation

148 during larval stages, we named this gene *apnoia* (*apn*). *apn* mutant animals

149 die as second instar larvae with dorsal trunks displaying reduced axial growth

150 and impaired apical surface area expansion, resulting in shorter tubes. This

151 phenotype is correlated with the absence of Crb from the apical surface. RNAi

152 knock-down of *crb* phenocopies the *apn* mutant phenotype of impaired

153 longitudinal growth. These results identify Apn as the first regulator of tracheal

154   tube growth in the larvae, which acts through Crb to control tube axial tube

155   expansion.

156

157

Results

Apnoia is an apical transmembrane protein expressed in *Drosophila* tracheae

To identify novel interactors of Crb, we searched for binding partners using a modified yeast two-hybrid screen (MBmate Y2H) [42,43] allowing bait and prey to interact at the yeast plasma membrane. The bait consisted of the most C-terminal extracellular EGF (epidermal growth factor)-like repeat, the transmembrane domain and the cytoplasmic tail of *Drosophila* Crb. One of the Crb interacting clones contained a 414bp cDNA insert representing the full-length transcript encoded by CG15887. Based on the tracheal inflation phenotype described below we named the gene *apnoia* (*apn*) (άπνοια, Greek for: lack of air).

The *apn mRNA* encodes a single protein isoform of 137 amino acids. Apn is predicted to contain a signal peptide at the amino terminus (1-23 aa) and two transmembrane domains (amino acids 50-72 and 79-101), based on the TMHMM transmembrane algorithm [44] prediction. Both the amino and carboxy terminus are located extracellularly, separated by a small intracellular loop (Suppl. Fig. S1). The PFAM algorithm (PFAM domains database 27.0) predicts that Apn contains two LPAM domains (47-56 aa and 78-90 aa), known as prokaryotic membrane lipoprotein lipid attachment site. Apn is highly conserved within the insect order (Suppl. Fig. S1) but does not appear to have a true orthologue in vertebrates.

To determine the tissue distribution and subcellular localization of *apn* mRNA and protein we performed *in situ* hybridizations and immunostainings of wild-type or transgenic animals, which either carried the *fosapn_{sfGFP}*, a

fosmid encoding the Apn protein C-terminally tagged with superfolded (sf) GFP [45], or a UAS-transgene encoding fluorescently-tagged Apn (UAS-$apn_{mCitrine}$). In addition, anti-Apn antibodies were raised in rabbits against a peptide of the N-terminal extracellular domain (aa 24-40). Expression of both *apn* mRNA (Fig. 1 A-C) and Apn protein (Fig. 1D-F and Suppl. Fig. S2A, B) was first detected in embryos at stage 13 in tracheal fusion cells. During embryonic stages 15 and 16, expression could also be detected in the dorsal and lateral trunks, in the visceral and dorsal branches and in the transverse connective branches. In the larvae, Apn is continuously expressed in the entire tracheal system (Suppl. Fig. S2C, D). As shown by antibody staining or $Apn_{mCitrine}$ fluorescence, Apn is restricted to the apical plasma membrane, where it co-localizes with the apical markers Stranded at second (Sas) (Fig. 1G-G'' and cross section in G''') and Uninflatable (Uif) (Fig. 1H-H'' and cross section in H'''). Apn co-localizes with Crb in the subapical region, a small region of the apical membrane apical to the adherens junctions (AJ) (Fig. 1I-I'' and cross section in I''').

This co-localization and the interaction in the yeast 2-hybrid system (Suppl. Fig. S2E) prompted us to further analyze the interaction between Apn and Crb in co-immunoprecipitation experiments. Full-length Apn (Apn^{FL}) expressed in $S2R^+$ cells co-immunoprecipitated full-length Crb (Crb^{FL}) (Fig. 1J). *In situ* interactions between Crb and Apn were corroborated by Proximity Ligation Assays (PLA) [46] using the fosmid line (*fosapn$_{sfGFP}$*). We found that Crb and Apn-sfGFP interact in the larval tracheae (Fig. 2A-A'', D-D'' and C), whereas no interaction between Apn and *D*Ecad-GFP (negative control) was detected (Fig. 2B-B'', E-E'' and C), indicating that the observed signal was

208   specific for the Crb-Apn interaction. To exclude any random interactions

209   between Crb and Apn in the apical domain we have tested a different apical

210   protein (SAS-Venus)[47] for its interaction with Apn and found no increased

211   PLA signal as compared to the signal between Crb and Apn (Fig. 2F-F"and G-

212   G").

213

214   ***apnoia* is required for tracheal tube growth**

215   To address possible functions of *apn* in tracheal development, we

216   generated a knockout line by CRISPR-Cas9, in which the open reading frame

217   of *apn* was replaced by DsRed (*apn¹*). No Apn protein could be detected with

218   the anti-Apn antibody in homozygous *apn¹* mutant larvae and embryos

219   (Suppl. Fig. S2B, D, F). In addition, no interaction between Crb and Apn was

220   detected in *apn¹* mutant tracheae in PLA assays as compared to wild type

221   tracheae (Suppl. Fig. S2G-G').

222   *apn¹* mutant tracheae displayed wild type morphology in all embryonic

223   stages, even in embryos derived from *apn¹* mutant germ line clones (Suppl.

224   Fig. S2H). However, *apn¹* mutant larvae died at second instar with reduced

225   body size and unusually twisted and uninflated tracheal tubes (compare Fig.

226   3A and B, Suppl. Fig. S2I, K). The phenotype is mostly manifested in the

227   posterior tracheal metameres 9 (Tr9) and 10 (Tr10). Similar phenotypes were

228   observed in larvae that carry *apn¹* in trans to Df(3R)Exel8158 (Suppl. Fig.

229   S2J), a chromosomal deletion that includes the *apn* locus, as well as in larvae

230   upon knock-down of *apn* by RNAi in the tracheae (Fig. 3C and Suppl. Fig.

231   S2K and S3A, B). In addition, the length of the dorsal trunk was significantly

232   reduced, as revealed by measurements of the posterior metamer length (Fig.

233   3E, F, H) The morphological and growth defects were rescued by one copy of

234   a fosmid containing the complete *apn* locus (fos*apn*mCherry.NLS) (Fig. 3D, G, H),

235   whereas a cDNA of Apn expressed in the tracheae rescued the phenotype in

236   only 20% of the larvae (compare Suppl. Fig. S3A, D and C, F).

237   The uninflated tubes observed in *apn1* deficient animals suggested

238   defects in tracheal maturation. In wild-type embryos as well as in each molting

239   step of larval development, tracheal maturation is characterized by distinct

240   sequential processes: i) secretion of a chitinous apical extracellular matrix

241   (aECM) into the lumen, which confers rigidity to the tube and is responsible

242   for tube expansion; ii) a pulse of endocytosis, resulting in the removal of

243   luminal proteins, and iii) liquid clearance and air filling [16,48]. Electron

244   micrographs of *apn1* mutant larvae revealed a disorganized lumen with

245   "tongues" of cellular protrusions into the lumen (Suppl. Fig. S3G, H). This

246   phenotype is probably a consequence of the irregularly twisted tubes

247   (compare Fig. 3I, J) and not due to defects in cuticle organization, since the

248   two different cuticular layers, epicuticle and procuticle, were normally formed

249   and the spaced thickenings formed by the aECM (taenidia) [49] appeared

250   similar to that of wild type tubes (Fig. 3I, J and Suppl. Fig. S3G', H'). This

251   conclusion is further supported by the normal expression of Dumpy (Dp) and

252   Piopio (Pio), two zona pellucida (ZP) domain proteins secreted into the lumen

253   [50,51] (Suppl. Fig. S3I-J'). The second maturation step, endocytosis of

254   luminal proteins, was also not impaired in *apn1* mutant tubes either. Using the

255   heterologous secreted mCherry-tagged protein ANF (UAS-ANF-mCherry, a

256   rat Atrial Natriuretic Factor) [52] revealed normal secretion and endocytosis in

257   tracheal cells deficient for *apn1* (compare Suppl. Fig. S3 K-L'). However, the

258 last maturation steps, liquid clearance and gas filling, were strongly affected in

259 *apn¹* mutant tracheae (compare Fig. 3K, K' and L, L'). We could exclude

260 leakage of the septate junctions (SJ) and hence loss of paracellular barrier as

261 a cause of this phenotype, since Contactin (Con) and Discs Large (Dlg), two

262 SJ components [53,54] were properly localized in the tracheae of *apn¹*

263 mutants (Suppl. Fig. S3M-N').

264 　　　　　Taken together, our data demonstrate that loss of *apn* affects late

265 steps of tracheal tube maturation, including liquid clearance and gas filling,

266 and impairs growth and morphology of the dorsal trunk at the second larval

267 stage.

268

269

270 **Apn supports apical membrane growth in larval tracheae**

271 　　　　　A striking defect observed in *apn¹* mutant larvae was a reduction in the

272 length of the dorsal trunk (Fig. 3E-H). To determine the cellular basis of this

273 phenotype we stained for *Drosophila* E-cadherin (*D*E-Cad) to visualize the cell

274 outline. We could not detect significant differences in cell number within

275 different metameres (data not shown). This led us to hypothesize that

276 shortening of tracheal tubes is caused by defective apical cell surface

277 expansion. Therefore, we measured the long and the short axes of cells

278 (referred to as axial and circumferential length, respectively) (see Fig. 4A) as

279 well as their cell surface area. While the circumferential cell length was not

280 significantly different, the axial cell length of *apn¹* mutants was reduced in

281 comparison to that of wild type cells (Fig. 4A, B and E, F). This difference was

282 also reflected by a reduced aspect ratio of the two axes (axial to

283 circumferential length) (Fig. 4G) and the overall reduction of the apical surface

284 area (Fig. 4C, D, H). From these results we conclude that Apn is required for

285 anisotropic apical surface expansion and hence tracheal tube elongation.

286

287 **Apnoia is required for maintenance of Crumbs on the apical membrane**

288 **of tracheal cells**

289   Regulation of apical cell surface area during axial growth of tracheal

290 tubes has been shown to require junctional and polarity proteins as well as

291 the apical protein Uif [55-58]. Therefore, to better understand the mechanism

292 by which *apn* ensures apical membrane growth, we examined the subcellular

293 distribution of junctional and polarity proteins in the tracheae of *apn^1* mutants.

294 The AJ markers Armadillo (Arm), the *Drosophila* β-catenin [59] (Fig. 5A, B),

295 Polychaetoid (Pyd), the single *Drosophila* ZO-1 orthologue [60] (Fig. 5C, D)

296 and *D*E-Cad (Fig. 5E, F) localized similar as in wild type tracheae. *apn^1*

297 mutant tracheal cells also showed normal distribution of Uif (Fig. 5G, H).

298 These results indicate no major defects in apico-basal polarity and epithelial

299 integrity of the tracheal tube in *apn^1* mutant larvae. The physical interaction

300 between Apn and Crb motivated us to analyze the expression of Crb in *apn^1*

301 mutants. In wild type tracheal cells of second instar larvae, Crb is localized in

302 the subapical region, outlining the cell (Fig. 5I). In contrast, Crb strongly

303 accumulated in cytoplasmic vesicles of multicellular, autocellular and

304 seamless tubes in *apn^1* mutant tracheae and upon knock-down of *apn* (Fig.

305 5J, R and Suppl. Fig. S4A-D'). Consistent with these results, not only

306 multicellular, but also autocellular and seamless tubes were twisted and

307 uninflated (Suppl. Fig. S4E-F'). However, the total protein levels of Crb were

13

308 unchanged as revealed by western blotting (Suppl. Fig. S2F). To investigate

309 whether *apn* is required for Crb apical localization only in the trachea we

310 analyzed another epithelial tube, the salivary glands. A uniform apical

311 localization of Crb was observed in both wild type and *apn¹* mutant salivary

312 glands indicating a tracheae-specific role of *apn* (Fig. S4H-I').

313 Similar as Crb, Stardust (Sdt) (Fig. 5K, L) and Moesin (Moe) (Fig. 5M,

314 N), whose subapical localization depends on Crb in many epithelia [61-64],

315 are found in the same vesicular compartments as Crb. The introduction of one

316 copy of the *apn* genomic locus (fos*apn*mCherry.NLS) into the *apn¹* mutant

317 background restored Crb membrane localization and suppressed the

318 accumulation of Crumbs loaded vesicles (CLVs) (Fig. 5O-Q). These results

319 indicate that Apn is required for Crb trafficking to or maintenance at the

320 plasma membrane of tracheal cells.

321 In order to distinguish between these two possibilities, we blocked

322 endocytosis in *apn¹* mutant tracheae chemically and genetically. After 2 hours

323 incubation with dynasore, an inhibitor of Dynamin [65], Crb was mostly

324 localized at the plasma membrane in *apn¹* mutant tracheal cells (Fig. 6A). In

325 contrast, *apn¹* mutant cells incubated with dynasore-free medium showed only

326 punctate staining of Crb (Fig. 6B). To corroborate this result, we blocked

327 endocytosis by using *shibire*^{ts1} (*shi*^{ts1}), a temperature sensitive allele of *shi*,

328 which encodes Dynamin. When incubated at the restrictive temperature

329 (34°C) *shi*^{ts1}*;apn¹* double mutant tracheae retained Crb at the apical plasma

330 membrane (Fig. 6C), as compared to *shi*^{ts1}*;apn¹* mutant tracheae, incubated

331 at the permissive temperature (25°C) (Fig. 6D). From these results we

332 concluded, that Apn is required for Crb maintenance at the apical membrane.

333	A striking feature of the *apn[1]* mutant phenotype is the accumulation of

334	Crb in intracellular vesicles (Fig. 5I, P). To determine their identity, we

335	analyzed components of the trafficking machinery, including markers for

336	endosomes, lysosomes and retromer. No major co-localization was observed

337	between CLVs and the early endosomal markers Rab5 (Fig. 7A-A") and Hrs

338	(Suppl. Fig. S5A-A") or Rab11, a marker for the recycling endosome (Fig. 7B-

339	B"). Interestingly, 25% of CLVs were also positive for the late endosomal

340	marker Rab7 (Fig. 7C-C"). No major overlap was found between vesicular Crb

341	and Lamp1 [66] or Arl8 [67], two markers of the lysosome (Suppl. Fig. S5B-B"

342	and C-C"). Strikingly, about 79% of CLVs co-localized with the retromer

343	component Vps35 (Fig. 8A-A").

344	We noticed that the majority of Vps35-positive vesicles were

345	significantly larger in *apn[1]* mutants, measuring around 0.7 µm (n=194

346	vesicles) in diameter, as compared to 0.27 µm (n=152 vesicles) in control

347	larval tracheal cells (Fig. 8B). No significant size differences in two other

348	trafficking compartments, such as the Arl8- (lysosomal) and the Golgin245-

349	(*trans*-Golgi) [68] positive vesicles, were observed between the two genotypes

350	(Fig. 8C, D). This result suggests that the size increase specifically in the

351	Vps35-positive compartment is an aspect of the *apn[1]* mutant phenotype.

352	Taken together, these results suggest that Apn maintains apical Crb by

353	preventing its clathrin-dependent endocytosis. Loss of *apn* results in Crb

354	accumulation in Vps35/retromer-positive vesicles of increased size.

355	

356	**Tracheal defects caused by *apn* depletion are mediated by *crb***

357   Since loss of apical Crb is often associated with reduced apical

358   membrane [28,69,70] and Crb is depleted from the apical membrane in *apn1*

359   mutant tracheal cells, we asked whether the impaired apical surface growth

360   observed in *apn1* mutant tracheae is due to its effect on apical Crb. Since

361   homozygous *crb* mutant embryos die with severe defects in many epithelia,

362   including the tracheae [24,71], we knocked-down *crb* in tracheal tubes by

363   expressing *crb* RNAi ubiquitously (using *da*-Gal4) or specifically in the

364   tracheae (using *btl*-Gal4). This resulted in a strong depletion of Crb and its

365   binding partner Sdt (Fig. 9A, B and A', B'), but had no effect on Apn

366   expression and localization (Fig. 9C, D and C', D'). RNAi-mediated

367   downregulation of *crb* reproduced several aspects of the *apn1* mutant

368   phenotypes, such as twisted tracheal tubes, lack of gas filling (Fig. 9E-H) and

369   reduced apical surfaces of tracheal tube cells (Fig. 9I-K). No defect in apico-

370   basal polarity was observed upon knockdown of Crb (Fig. 9I, J and I", J"). In

371   addition, most animals died at L2 (larval stage 2) with some surviving until L3

372   (larval stage 3) instar larvae.

373   To assess whether the increased size of Vps35 positive vesicles in

374   *apn1* mutants are due to Crb accumulation in these vesicles, we knocked-

375   down *crb* in *apn1* tracheae using *btl*-Gal4. We found a small, yet significant

376   reduction in the size of Vps35 positive vesicles in *apn1* tracheal cells upon *crb*

377   RNAi expression, compared to that of *apn1* single mutants (Fig. 10A, B, D and

378   Suppl. Fig. S6A-C). In contrast, Vps35 positive vesicles in tracheal cells

379   expressing *crb* RNAi in otherwise wild-type animals are comparable in size to

380   those of wild type Vps35 vesicles (compare Fig. 10C, D and Fig. 8B).

381   These results are the first to show that loss of *crb* results in a reduction

382   of the apical surface area of larval tracheal cell, which in turn prevents proper

383   tube elongation. In addition, they identify Apn as a novel regulator of apical

384   Crb in the developing tracheae, which controls dorsal trunk maturation and

385   expansion. Absence of *apn* leads to accumulation of Crb in Vps35 positive

386   vesicles, which may contribute to the increase in vesicular size.

387

Discussion

389   This work identifies Apn as the first protein essential for airway

390   maturation in *Drosophila* larval stages. Apn is expressed apically in tracheal

391   epithelial cells, where it co-localizes and physically interacts with Crb. *apn^1*

392   mutant larvae exhibit loss of tracheal tissue structure, manifested by tube size

393   defects and impaired gas filling, resulting in body size reduction and lethality

394   at second instar. At the cellular level, exclusion of Crb from the apical

395   membrane in *apn^1* mutant larval tracheae goes along with apical cell surface

396   reduction and an overall tracheal tube shortening. Absence of *apn* leads to

397   Crb inhibition and accumulation in enlarged, Vps35/retromer-positive vesicles.

398   Elongation of the tracheal tube has been extensively studied in

399   embryos where it has been shown to rely on different mechanisms, such as

400   the organization of the aECM and cell shape changes [33,72-76]. Anisotropic

401   growth of the apical plasma membrane is an additional mechanism to achieve

402   proper longitudinal tube expansion. However, only few proteins have been

403   described so far to regulate this process. One of these, the protein kinase

404   Src42A, is required for the expansion of the cells in the axial direction, and

405   loss of *Src42A* function results in tube length shortening, which is associated

406 with an increased tube diameter [72,75,77]. Src42A has been suggested to

407 exert its function, at least in part, by controlling *D*E-cadherin recycling and

408 hence adherens junctions remodeling [72] and/or by its interaction with the

409 Diaphanous-related formin *d*DAAM (*Drosophila* D̲ishevelled-a̲ssociated

410 a̲ctivator of m̲orphogenesis), loss of which results in reduced apical levels of

411 activated pSrc42A [75]. More recently, Src42A has been suggested to control

412 axial expansion by inducing anisotropic localization of Crb along the

413 longitudinal junctions in comparison to transverse junctions [78]. However, we

414 never observed any anisotropic distribution of Crb in wild type larval tracheal

415 cells, making it unlikely that at this developmental stage, axial expansion is

416 regulated by a Src42A-dependent mechanism. This assumption is

417 corroborated by the observation that, unlike in *Src42A* mutants, the lack of

418 longitudinal expansion in *apn[1]* mutant larval tubes is not associated with

419 circumferential expansion. Another protein regulating tube elongation in the

420 embryo is the epidermal growth factor receptor, EGFR. Expressing a

421 constitutively active EGFR results in shortened tracheal tubes with smaller

422 apical cell surfaces, but with increased diametrical growth. In this condition,

423 Crb shows altered apical distribution [78,79]. This phenotype differs from the

424 *apn[1]* phenotype, where apical localization of Crb is almost completely lost and

425 only longitudinal tube growth is affected. This suggests that Apn executes

426 tube length expansion by a different mechanism.

427 How does decrease in tubular growth lead to loss of tracheal structure?

428 During development, the larval body, including the tracheal tissue, elongates

429 about 8-fold [18]. Impaired axial tracheal cell growth in *apn[1]* mutants thus may

430 affect the balance between the forces exerted by the apical membrane growth

431 on the one hand and the resistance provided by the luminal aECM on the

432 other, an important mechanism described previously to control tube shape in

433 the embryo [33]. This could lead to physical rupture of tubes mutant for *apn1*,

434 allowing fluid entry. The presence of fluid would, in turn, disrupt proper gas

435 filling, resulting in hypoxia and, consequently, in impaired body growth.

436 Several studies have shown that in some tissues Crb accumulation on

437 the apical membrane is mediated by the retromer complex, which controls

438 either the retrograde transport of Crb to the *trans*-Golgi [80] or the direct

439 trafficking from the endosomes to the plasma membrane [39,41,79]. The

440 physical interaction of Apn and Crb, the functional requirement of Apn for Crb

441 apical localization and the fact that in *apn1* mutants Crb is trapped in Vps35-

442 positive/retromer vesicles all suggest that Apn is required for trafficking and/or

443 maintenance of Crb at the apical membrane (Fig. 11).

444 However, the increase in the size of Vps35-positive vesicles in *apn1*

445 mutant cells, which is, to some extent, due to the accumulation of Crb,

446 suggests defects in retromer function, which may prevent Crb lysosomal

447 degradation. Further studies will help to elucidate at which level Apn controls

448 Crb trafficking in larval tracheae.

449

450 **Materials and Methods**

451 **Fly stocks**

452 Flies were maintained at 25°C with 50% humidity unless stated

453 otherwise. The fos*apn*sfGFP (tagging with 2XTY1-SGFP-V5-preTEV-BLRP-

454 3XFLAGdFRT was done C-terminally) and fos*apn*mCherry.NLS (tagging with ubi-

455 mCherry-NLS-T2A was done N-terminally) were provided by the Flyfos library

456   at MPI-CBG [45]. The following fly lines were used: Rab5-YFP, Rab7-YFP

457   and   Rab11-YFP   (http://rablibrary.mpi-cbg.de/cgi-bin/rab_overview.pl)   [81]

458   (kindly provided by Marko Brankatschk), UAS-moe-GFP (kindly provided by

459   Brian Stramer) [82], UAS-ANF-mCherry (modified from [52]), and w; *D*E-

460   Cad::GFP [83], w; Sas:: Venus [47], w; btl-Gal4 [84]. The following fly stocks

461   were obtained from the Bloomington *Drosophila* Stock Center (BDSC): y[1]

462   M{w[+mC]=nos-Cas9.P}ZH-2A w[*]   (BDSC, #54591), *shi*[ts1] (BDSC, #7068),

463   y[1]   v[1];   P{y[+t7.7]   v[+t1.8]=TRiP.HMS01842}attP40   (*crb*[RNAi])   (BDSC,

464   #38373),   w[1118];da[G32]-Gal4   (BDSC,   #55851)   [21],   w[1118];

465   Df(3R)Exel8158/TM6B, Tb (BDSC, #7974) and UAS-lamp1-GFP (BDSC,

466   #42714). The CG15887 (*apn*[RNAi]) (VDRC, #9070) was obtained from the

467   Vienna *Drosophila* Resource Center.

468

469   **Generation of *apn*[1] mutant allele by CRISPR/Cas9**

470   Target sites were designed using the settings of the flyCRISPR

471   Optimal Target Finder (http://tools.flycrispr.molbio.wisc.edu/targetFinder/), to

472   guide Cas9 to two target sites, one at the 5'UTR (gagggtctgggccggcttacTGG)

473   and one at the 3'UTR end (gcaaagtcacggagaaatctGGG) (UPPERCASE:

474   PAM) of CG15887 (*apn*), with the aim to delete the whole Open Reading

475   Frame. The following phosphorylated DNA oligomers were used as primers

476   for   PCR,   using   10ng   of   pCFD4-U6:1U6:3tandem   gRNAs   as   template

477   (Addgene   #49411;[85]):   forward   primers   5'-[P]-

478   tatataggaaagatatccgggtgaacttcgGCAAAGTCACGGAGAAATCTgttttagagctaga

479   aatagcaag-3',   reverse   primer   5'-[P]-

480   attttaacttgctatttctagctctaaaacGTAAGCCGGCCCAGACCCTCcgacgttaaattgaa

481 aataggtc-3'. The resulting DNA fragment was cloned into pCFD4-

482 U6:1U6:3tandemgRNAs via Gibson Assembly after linearization of the vector

483 with BbsI. To replace the CG15887 ORF with 3XP3-dsRed we used the pHD-

484 DsRed-attP vector (Addgene #51019;[86]). The homology arms necessary to

485 obtain Homology Directed Repair were sequences covering 1kb regions of

486 upstream and downstream of 5'UTR and 3'UTR gRNA cut sites, respectively.

487 Cloning into the vector was obtained with AarI for the 5'-homology arm (5'-HA)

488 and SapI for the 3'-homoly arm (3'-HA). Primer sequences are: Forward

489 primer   5'-HA   (5'-

490 TGTACACCTGCGAATTCGCCCACACTGTTTGGCATCTGGCGGCGCTCCT

491 CC-3'),   Reverse   primer   5'-HA   (5'-

492 TGTACACCTGCAGATCTACTTTCTCCGTGACTTTGCTCATAGCTCATTAT

493 GG-3'),   Forward   primer   3'-HA   (5'-

494 GCTAGCTCTTCGTATTACTGGGCGGCTACTTGAAATTCGGGAGCC-3'),

495 Reverse   primer   3'-HA   (5'-

496 GCTAGCTCTTCGGACCCCCAATAACATGTCCGTCCGCACTACG-3').

497 Homology arm sequences were amplified from the BAC genomic clone

498 BACR05K08 (obtained from BACPAC resources center (BPRC). The two

499 plasmids were injected in a concentration of 400ng each, into nos::Cas9

500 embryos [85].

501

502 **Generation of transgenic flies**

503 To generate the UAS-*apn* transgenic line, the CG15887 (*apn*) cDNA

504 (RE53127; obtained from DGRC) was cloned into pJFRC-MUH-mCitrine[87]

505 by BglII-NotI using standard molecular biology techniques. Plasmid constructs

506 were injected by BestGene.

507

Dynasore treatment of larval tracheae

509 *apn1* mutant tracheae from second instar larvae were dissected in

510 Grace's medium supplemented with Pep/Strep. Tissues were incubated in

511 60µM dynasore (Enzo Life Sciences) in Grace's medium containing Pep/Strep

512 and 2.5% FCS at room temperature for 2hr. The dynasore was washed out

513 and tracheae were fixed in 4% FA in Grace's medium for 30min.

514

Yeast-two-Hybrid screen

516 Part of the coding sequence of a *Drosophila melanogaster crb* cDNA

517 (encoding aa: 2034-2189) (GenBank accession number NM_001043286.1)

518 was PCR-amplified and cloned in pB102, in frame with the STE2 leader

519 sequence at the N-terminus and ubiquitin (Cub) at the C-terminus of the bait

520 which is coupled to the artificial transcription factor LexA-VP16 (STE2-Crb-

521 Cub-LexA-VP16). The construct was checked by sequencing. Prey fragments

522 were isolated from an MBmate screen with *Drosophila melanogaster* Crb as

523 bait against a *Drosophila* Embryo NubG-x (D3DE_dT) library (NubG stands

524 for the N-terminal domain of mutated ubiquitin and x for the prey fragment).

525 Interaction pairs were tested in duplicate as two independent clones. For each

526 interaction, several dilutions (undiluted, 10^{-1}, 10^{-2}, 10^{-3}) of the diploid yeast

527 cells (culture normalized at 5Å~107 cells) and expressing both bait and prey

528 constructs were spotted in selective media. The DO-2 selective medium

529 lacking tryptophan and leucine was used to control for growth and to verify the

presence of both the bait and prey plasmids. The different dilutions were also

spotted on a selective medium without tryptophan, leucine and histidine (DO-

3). Six different concentrations of 3-AT, an inhibitor of the HIS3 gene product,

were added to the DO-3 plates to increase stringency and reduce possible

auto activation. The following 3-AT concentrations were tested: 1, 5,10, 50,

100 and 200 mM. The 1-by-1 Yeast two-hybrid assays were performed by

Hybrigenics Services, S.A.S., Paris, France (http://www.hybrigenics.com)

Cell Culture and Transfection

Drosophila S2R$^+$ cells were cultured at 25 °C in Schneider's *Drosophila*

medium (Sigma) supplemented with 10% fetal bovine serum. p*Act5*-Gal4

together with UAS-Apn^{FL} and/or UAS-Crb^{FL} [21] (encoding full-length Apn and

Crb, respectively) was transfected into S2R$^+$ cells using FuGENE HD

(Promega) according to the manufacturer's protocol.

Immunoprecipitation

Transfected cells were harvested after 48 h, washed with ice-cold PBS

(120 mM NaCl in phosphate buffer at pH 6.7), resuspended in lysis buffer

(containing 10% glycerol; 1% Triton X-100; 1.5 mM MgCl$_2$; 120 mM NaCl; 100

mM PIPES, pH 6.8; 3 mM CaCl$_2$; 1 mM PMSF and Complete^{TM}). Cells were

lysed on ice for 20min and lysates were spinned at 14.000 rpm for 20min at

4°C. The supernatant was incubated with the antibody for 2 hours. In the

meantime 50µl of Protein G were washed 3 times with blocking solution and

incubated with the antibody solution overnight at 4°C. Protein G beads were

collected by centrifugation for 2 min at 3.000rpm and washed 4 times with

555 lysis buffer. Beads were resuspended in 1.5x SDS sample buffer and heated

556 for 5min at 95°C.

557

558 **Western Blot**

559   Wild-type and apn^1 mutant embryos and dissected larval tracheae

560 were homogenized on ice using a Dounce tissue grinder in 1ml of lysis buffer

561 containing 130mM NaCl, 50mM Tris-HCL pH=8, 0,5% Triton-X and protease

562 inhibitor (Roche). After 30min at 4°C under rotation the homogenate was

563 centrifuged for 20min at 14.000rpm. Sample buffer 3x SDS was added to the

564 supernatant and boiled for 5min at 95°C.

565   Proteins were separated by SDS-PAGE and blotted onto nitrocellulose

566 0.45 membrane (Amersham). After blocking in 5% BSA+TBST, the

567 membrane was incubated overnight with rabbit anti-Apn diluted 1:1000, rat

568 anti-Crb[88] diluted 1:1000 and mouse anti-alpha-tubulin (Sigma) diluted

569 1:5000 in blocking buffer. Peroxidase antibodies were used for detection.

570

571 **Proximity Ligation assay (PLA)**

572   Tracheae from $fosapn_{sfGFP}$ third instar larvae were dissected and fixed

573 in ice cold 4% FA in PBS. Primary antibodies against GFP (rabbit anti-GFP

574 1:250; Invitrogen A11122) and Crb (rat anti-Crb 1:500 [88]) were added and

575 incubated overnight at 4°C. The Duolink PLA Kit (Sigma Aldrich) was used to

576 incubate the tissue with the PLA probes PLUS and MINUS at 37°C for 1 hour.

577 Ligation of the PLA oligonucleotides and amplification were performed at

578 37°C for 30 min and 100min, respectively. Samples were mounted in Duolink

579 mounting media and imaged using Zeiss LSM 880.

580

Generation of Apn antiserum

Polyclonal antibodies against CG15887 were raised in rabbits using the KLH-conjugated synthetic peptide QQAANSSDSDSDVAESC (from the N-terminal extracellular part) for immunization. Antibodies were subsequently affinity-purified using the same peptide immobilized on SulfoLink Coupling Gel (ThermoFisher #20401) and following recommendations by the manufacturer. The work was performed by the MPI-CBG Antibody Facility.

588

Immunohistochemistry

Immunostainings on embryos were done as follows: embryos were dechorionated in 50% bleach for 2min and fixed for 20min in formaldehyde/heptane mixture. After devitellinization in methanol, embryos were permeabilized in 0.1% Triton X-100/PBS except for rabbit anti-Apn staining, for which embryos were permeabilized in 0.2% Saponin/ PBS. After washing, embryos were incubated for 1h at RT in blocking solution [(0.5%w/v BSA in PBST/S (0.1%v/v Triton X-100) or (0.2%w/v Saponin)]. Second instar larvae were opened in PBS and fixed in 4% formaldehyde for 20min. After washing in either 0.1% Triton X-100/PBS or 0.2% Saponin/ PBS (for anti-Apn antibody staining), tracheae were dissected and incubated in blocking solution for 1h at RT. Embryos and tracheae were incubated in primary antibodies overnight at 4°C, washed and incubated with secondary antibody for 2h at RT. Samples were mounted in Vectashield (Vector Laboratories) and imaged with LSM 880 Laser Scanning Confocal Microscope (Carl Zeiss). Unless otherwise indicated, images shown are z-stack projections of sections.

605   Images were processed with Fiji software [89]. Cell area measurements were

606   obtained by using the Fiji Freehand selection tool.

607   The following primary antibodies were used: rabbit anti-Apn (1:500-1:1000)

608   (this study), rabbit or rat anti-Crb (1:1000) [21,24,88], rabbit anti-Sdt (1:1000)

609   [61], guinea pig anti-Cont (1:1500; gift from Manzoor Bhat), guinea pig anti-Uif

610   (1:20; gift from Robert Ward), mouse anti-Pyd (1:1000; gift from Alan

611   Fanning), rabbit anti-Pio (1:50; gift from Markus Affolter), guinea pig anti-HRS

612   and anti-Vps26 (1:20 and 1:1000, respectively; gift from Hugo Bellen), rabbit

613   anti-SAS (1:500 gift from Douglas Cavener), goat anti Golgin245 (1:200,

614   DSHB), mouse anti-Arm (1:50, DSHB, N27A1), rabbit anti-Arl8 (1:100,

615   DSHB), rat anti-*D*E-Cad (1:50, DSHB, DCAD2), mouse anti-Dlg (1:500,

616   DSHB, 4F3), rabbit anti-GFP A11122 (1:250, Thermo Fischer), mouse anti-

617   GFP (1:250, Roche), Chitin binding probe-633 (1:20; gift from Maria

618   Leptin)[90]. The secondary antibodies Alexa Fluor 488, 568 and 633

619   (Molecular Probes) were used at 1:400 dilution.

620

621   **RNA *in situ* hybridization**

622   DIG-labelled RNA probes were synthesized from PCR templates amplified

623   from for a full-length *apn* (RE53127) cDNA clone. Sequence specific primers

624   for pFLC-I vector (BDGP resources) were: M13 (-21) 5'-

625   TGTAAAACGACGGCCAGT-3'   and   M13   (REV)   5'-

626   GGAAACAGCTATGACCATG-3'. PCR products were purified by PCR

627   purification columns (Promega, PCR CleanUp system). *In vitro* transcription

628   reactions were performed by mixing the PCR product with the polymerase

629   mix, which includes T3 RNA polymerase. RNA was labelled with digoxigenin-

630 UTP (Roche Applied Science # 11277073910). Eggs were collected on apple

631 juice plates for 12h. Embryos were dechorionated in 50%bleach for 2min and

632 fixed for 20min in formaldehyde/heptane mixture. After devitellinization in

633 methanol embryos were processed for hybridization modified from [91].

634

635

Electron microscopy analysis

636

637   Larvae were fixed in 2% Glutaraldehyde in 0.1M PB buffer pH 7.2 for

638   20min at room temperature. Larvae were transferred in microcentrifuge tubes

639   and fixed in 1%OsO$_4$/2% Glutaraldehyde and then 2% OsO$_4$. Further

640   procedures were done according to the protocol described [92]. Ultrathin

641   sections of 0.1µm were prepared and analyzed with Tecnai 12 BioTWIN (FEI

642   Company).

643

644   **Image analysis**

645   We developed a Fiji script to quantify the co-localization of proteins of

646   the trafficking machinery (e.g. retromer, lysosome, Golgi) with Crb-positive

647   vesicles. Two channel images showing fluorescent Crb signal and protein X

648   signal were imported into a script for the freely available Fiji software [89] and

649   characterized for their overlap. The plugin was tested on Fiji current version:

650   (Fiji is just ImageJ) ImageJ 2.0.0-rc-65/1.51w. The code of the scripts and its

651   documentation are available on the project repository (https://git.mpi-

652   cbg.de/bioimage-informatics/Skouloudaki_et_al_Crumbs_overlap_analysis).

653

654

References

1. Yeaman C, Grindstaff KK, Nelson WJ (1999) New perspectives on mechanisms involved in generating epithelial cell polarity. Physiol Rev 79: 73-98.
2. Honda H (2017) The world of epithelial sheets. Dev Growth Differ 59: 306-316.
3. Rodriguez-Boulan E, Macara IG (2014) Organization and execution of the epithelial polarity programme. Nat Rev Mol Cell Biol 15: 225-242.
4. Bernascone I, Hachimi M, Martin-Belmonte F (2017) Signaling Networks in Epithelial Tube Formation. Cold Spring Harb Perspect Biol 9.
5. Blasky AJ, Mangan A, Prekeris R (2015) Polarized protein transport and lumen formation during epithelial tissue morphogenesis. Annu Rev Cell Dev Biol 31: 575-591.
6. Iruela-Arispe ML, Beitel GJ (2013) Tubulogenesis. Development 140: 2851-2855.
7. Jewett CE, Prekeris R (2018) Insane in the apical membrane: Trafficking events mediating apicobasal epithelial polarity during tube morphogenesis. Traffic.
8. Davies JC, Alton EW, Bush A (2007) Cystic fibrosis. BMJ 335: 1255-1259.
9. Ganner A, Neumann-Haefelin E (2017) Genetic kidney diseases: Caenorhabditis elegans as model system. Cell Tissue Res 369: 105-118.
10. Harris PC, Torres VE (2009) Polycystic kidney disease. Annu Rev Med 60: 321-337.
11. Wilson PD (2011) Apico-basal polarity in polycystic kidney disease epithelia. Biochim Biophys Acta 1812: 1239-1248.
12. Lubarsky B, Krasnow MA (2003) Tube morphogenesis: making and shaping biological tubes. Cell 112: 19-28.
13. Maruyama R, Andrew DJ (2012) Drosophila as a model for epithelial tube formation. Dev Dyn 241: 119-135.
14. Beitel GJ, Krasnow MA (2000) Genetic control of epithelial tube size in the Drosophila tracheal system. Development 127: 3271-3282.

700 15. Zuo L, Iordanou E, Chandran RR, Jiang L (2013) Novel mechanisms of tube-
701   size regulation revealed by the Drosophila trachea. Cell Tissue Res 354:
702   343-354.
703 16. Hayashi S, Dong B (2017) Shape and geometry control of the Drosophila
704   tracheal tubule. Dev Growth Differ 59: 4-11.
705 17. Luschnig S, Uv A (2014) Luminal matrices: an inside view on organ
706   morphogenesis. Exp Cell Res 321: 64-70.
707 18. Glasheen BM, Robbins RM, Piette C, Beitel GJ, Page-McCaw A (2010) A matrix
708   metalloproteinase mediates airway remodeling in Drosophila. Dev Biol
709   344: 772-783.
710 19. Manning G, Krasnow MA (1993) Development of the Drosophila tracheal
711   system. In: Bate M, Martinez-Arias A, editors. The Development of
712   Drosophila: New York: Cold Spring Harbor Laboratory Press. pp. 609-685.
713 20. Whitten JM (1957) The Post-embryonic Development of the tracheal System
714   in Drosophila melanogaster. J Cell Science 41: 132-150.
715 21. Wodarz A, Hinz U, Engelbert M, Knust E (1995) Expression of crumbs confers
716   apical character on plasma membrane domains of ectodermal epithelia of
717   Drosophila. Cell 82: 67-76.
718 22. Grawe F, Wodarz A, Lee B, Knust E, Skaer H (1996) The Drosophila genes
719   crumbs and stardust are involved in the biogenesis of adherens junctions.
720   Development 122: 951-959.
721 23. Tepass U (1996) Crumbs, a component of the apical membrane, is required
722   for zonula adherens formation in primary epithelia of Drosophila. Dev
723   Biol 177: 217-225.
724 24. Tepass U, Theres C, Knust E (1990) crumbs encodes an EGF-like protein
725   expressed on apical membranes of Drosophila epithelial cells and
726   required for organization of epithelia. Cell 61: 787-799.
727 25. de Vreede G, Schoenfeld JD, Windler SL, Morrison H, Lu H, et al. (2014) The
728   Scribble module regulates retromer-dependent endocytic trafficking
729   during epithelial polarization. Development 141: 2796-2802.
730 26. Fletcher GC, Lucas EP, Brain R, Tournier A, Thompson BJ (2012) Positive
731   feedback and mutual antagonism combine to polarize Crumbs in the
732   Drosophila follicle cell epithelium. Curr Biol 22: 1116-1122.
733 27. Klebes A, Knust E (2000) A conserved motif in Crumbs is required for E-
734   cadherin localisation and zonula adherens formation in Drosophila. Curr
735   Biol 10: 76-85.
736 28. Laprise P, Beronja S, Silva-Gagliardi NF, Pellikka M, Jensen AM, et al. (2006)
737   The FERM protein Yurt is a negative regulatory component of the Crumbs
738   complex that controls epithelial polarity and apical membrane size. Dev
739   Cell 11: 363-374.
740 29. Lu H, Bilder D (2005) Endocytic control of epithelial polarity and
741   proliferation in Drosophila. Nat Cell Biol 7: 1232-1239.
742 30. Moberg KH, Schelble S, Burdick SK, Hariharan IK (2005) Mutations in
743   erupted, the Drosophila ortholog of mammalian tumor susceptibility gene
744   101, elicit non-cell-autonomous overgrowth. Dev Cell 9: 699-710.
745 31. Pellikka M, Tanentzapf G, Pinto M, Smith C, McGlade CJ, et al. (2002) Crumbs,
746   the Drosophila homologue of human CRB1/RP12, is essential for
747   photoreceptor morphogenesis. Nature 416: 143-149.

748   32. Tanentzapf G, Smith C, McGlade J, Tepass U (2000) Apical, lateral, and basal
749   polarization cues contribute to the development of the follicular
750   epithelium during Drosophila oogenesis. J Cell Biol 151: 891-904.
751   33. Dong B, Hannezo E, Hayashi S (2014) Balance between apical membrane
752   growth and luminal matrix resistance determines epithelial tubule shape.
753   Cell Rep 7: 941-950.
754   34. Letizia A, Ricardo S, Moussian B, Martin N, Llimargas M (2013) A functional
755   role of the extracellular domain of Crumbs in cell architecture and
756   apicobasal polarity. J Cell Sci 126: 2157-2163.
757   35. Zou J, Wang X, Wei X (2012) Crb apical polarity proteins maintain zebrafish
758   retinal cone mosaics via intercellular binding of their extracellular
759   domains. Dev Cell 22: 1261-1274.
760   36. Das S, Knust E (2018) A dual role of the extracellular domain of Drosophila
761   Crumbs for morphogenesis of the embryonic neuroectoderm. Biol Open 7.
762   37. Blankenship JT, Fuller MT, Zallen JA (2007) The Drosophila homolog of the
763   Exo84 exocyst subunit promotes apical epithelial identity. J Cell Sci 120:
764   3099-3110.
765   38. Lin YH, Currinn H, Pocha SM, Rothnie A, Wassmer T, et al. (2015) AP-2-
766   complex-mediated endocytosis of Drosophila Crumbs regulates polarity
767   by antagonizing Stardust. J Cell Sci 128: 4538-4549.
768   39. Pocha SM, Wassmer T, Niehage C, Hoflack B, Knust E (2011) Retromer
769   controls epithelial cell polarity by trafficking the apical determinant
770   Crumbs. Curr Biol 21: 1111-1117.
771   40. Roeth JF, Sawyer JK, Wilner DA, Peifer M (2009) Rab11 helps maintain apical
772   crumbs and adherens junctions in the Drosophila embryonic ectoderm.
773   PLoS One 4: e7634.
774   41. Zhou B, Wu Y, Lin X (2011) Retromer regulates apical-basal polarity through
775   recycling Crumbs. Dev Biol 360: 87-95.
776   42. Stagljar I, Korostensky C, Johnsson N, te Heesen S (1998) A genetic system
777   based on split-ubiquitin for the analysis of interactions between
778   membrane proteins in vivo. Proc Natl Acad Sci U S A 95: 5187-5192.
779   43. Dunkler A, Muller J, Johnsson N (2012) Detecting protein-protein interactions
780   with the Split-Ubiquitin sensor. Methods Mol Biol 786: 115-130.
781   44. Sonnhammer EL, von Heijne G, Krogh A (1998) A hidden Markov model for
782   predicting transmembrane helices in protein sequences. Proc Int Conf
783   Intell Syst Mol Biol 6: 175-182.
784   45. Sarov M, Barz C, Jambor H, Hein MY, Schmied C, et al. (2016) A genome-wide
785   resource for the analysis of protein localisation in Drosophila. Elife 5:
786   e12068.
787   46. Soderberg O, Gullberg M, Jarvius M, Ridderstrale K, Leuchowius KJ, et al.
788   (2006) Direct observation of individual endogenous protein complexes in
789   situ by proximity ligation. Nat Methods 3: 995-1000.
790   47. Firmino J, Tinevez JY, Knust E (2013) Crumbs affects protein dynamics in
791   anterior regions of the developing Drosophila embryo. PLoS One 8:
792   e58839.
793   48. Tsarouhas V, Senti KA, Jayaram SA, Tiklova K, Hemphala J, et al. (2007)
794   Sequential pulses of apical epithelial secretion and endocytosis drive
795   airway maturation in Drosophila. Dev Cell 13: 214-225.

796   49. Ozturk-Colak A, Moussian B, Araujo SJ (2016) Drosophila chitinous aECM and
797   its cellular interactions during tracheal development. Dev Dyn 245: 259-
798   267.
799   50. Jazwinska A, Ribeiro C, Affolter M (2003) Epithelial tube morphogenesis
800   during Drosophila tracheal development requires Piopio, a luminal ZP
801   protein. Nat Cell Biol 5: 895-901.
802   51. Bokel C, Prokop A, Brown NH (2005) Papillote and Piopio: Drosophila ZP-
803   domain proteins required for cell adhesion to the apical extracellular
804   matrix and microtubule organization. J Cell Sci 118: 633-642.
805   52. Rao S, Lang C, Levitan ES, Deitcher DL (2001) Visualization of neuropeptide
806   expression, transport, and exocytosis in Drosophila melanogaster. J
807   Neurobiol 49: 159-172.
808   53. Faivre-Sarrailh C, Banerjee S, Li J, Hortsch M, Laval M, et al. (2004)
809   Drosophila contactin, a homolog of vertebrate contactin, is required for
810   septate junction organization and paracellular barrier function.
811   Development 131: 4931-4942.
812   54. Woods DF, Hough C, Peel D, Callaini G, Bryant PJ (1996) Dlg protein is
813   required for junction structure, cell polarity, and proliferation control in
814   Drosophila epithelia. J Cell Biol 134: 1469-1482.
815   55. Behr M, Riedel D, Schuh R (2003) The claudin-like megatrachea is essential in
816   septate junctions for the epithelial barrier function in Drosophila. Dev Cell
817   5: 611-620.
818   56. Laplante C, Paul SM, Beitel GJ, Nilson LA (2010) Echinoid regulates tracheal
819   morphology and fusion cell fate in Drosophila. Dev Dyn 239: 2509-2519.
820   57. Wu VM, Schulte J, Hirschi A, Tepass U, Beitel GJ (2004) Sinuous is a
821   Drosophila claudin required for septate junction organization and
822   epithelial tube size control. J Cell Biol 164: 313-323.
823   58. Zhang L, Ward REt (2009) uninflatable encodes a novel ectodermal apical
824   surface protein required for tracheal inflation in Drosophila. Dev Biol 336:
825   201-212.
826   59. Peifer M, Orsulic S, Sweeton D, Wieschaus E (1993) A role for the Drosophila
827   segment polarity gene armadillo in cell adhesion and cytoskeletal
828   integrity during oogenesis. Development 118: 1191-1207.
829   60. Choi W, Jung KC, Nelson KS, Bhat MA, Beitel GJ, et al. (2011) The single
830   Drosophila   ZO-1   protein   Polychaetoid   regulates   embryonic
831   morphogenesis in coordination with Canoe/afadin and Enabled. Mol Biol
832   Cell 22: 2010-2030.
833   61. Bachmann A, Schneider M, Theilenberg E, Grawe F, Knust E (2001)
834   Drosophila Stardust is a partner of Crumbs in the control of epithelial cell
835   polarity. Nature 414: 638-643.
836   62. Medina E, Williams J, Klipfell E, Zarnescu D, Thomas G, et al. (2002) Crumbs
837   interacts with moesin and beta(Heavy)-spectrin in the apical membrane
838   skeleton of Drosophila. J Cell Biol 158: 941-951.
839   63. Hong Y, Stronach B, Perrimon N, Jan LY, Jan YN (2001) Drosophila Stardust
840   interacts with Crumbs to control polarity of epithelia but not neuroblasts.
841   Nature 414: 634-638.
842   64. Salis P, Payre F, Valenti P, Bazellieres E, Le Bivic A, et al. (2017) Crumbs,
843   Moesin and Yurt regulate junctional stability and dynamics for a proper

844   morphogenesis of the Drosophila pupal wing epithelium. Sci Rep 7:
845   16778.
846 65. Macia E, Ehrlich M, Massol R, Boucrot E, Brunner C, et al. (2006) Dynasore, a
847   cell-permeable inhibitor of dynamin. Dev Cell 10: 839-850.
848 66. Pulipparacharuvil S, Akbar MA, Ray S, Sevrioukov EA, Haberman AS, et al.
849   (2005) Drosophila Vps16A is required for trafficking to lysosomes and
850   biogenesis of pigment granules. J Cell Sci 118: 3663-3673.
851 67. Hofmann I, Munro S (2006) An N-terminally acetylated Arf-like GTPase is
852   localised to lysosomes and affects their motility. J Cell Sci 119: 1494-1503.
853 68. Riedel F, Gillingham AK, Rosa-Ferreira C, Galindo A, Munro S (2016) An
854   antibody toolkit for the study of membrane traffic in Drosophila
855   melanogaster. Biol Open 5: 987-992.
856 69. Johnson K, Grawe F, Grzeschik N, Knust E (2002) Drosophila crumbs is
857   required to inhibit light-induced photoreceptor degeneration. Curr Biol
858   12: 1675-1680.
859 70. Spannl S, Kumichel A, Hebbar S, Kapp K, Gonzalez-Gaitan M, et al. (2017) The
860   Crumbs_C isoform of Drosophila shows tissue- and stage-specific
861   expression and prevents light-dependent retinal degeneration. Biol Open
862   6: 165-175.
863 71. Tepass U, Knust E (1990) Phenotypic and developmental analysis of
864   mutations at thecrumbs locus, a gene required for the development of
865   epithelia inDrosophila melanogaster. Roux Arch Dev Biol 199: 189-206.
866 72. Forster D, Luschnig S (2012) Src42A-dependent polarized cell shape changes
867   mediate epithelial tube elongation in Drosophila. Nat Cell Biol 14: 526-
868   534.
869 73. Laprise P, Paul SM, Boulanger J, Robbins RM, Beitel GJ, et al. (2010) Epithelial
870   polarity proteins regulate Drosophila tracheal tube size in parallel to the
871   luminal matrix pathway. Curr Biol 20: 55-61.
872 74. Luschnig S, Batz T, Armbruster K, Krasnow MA (2006) serpentine and
873   vermiform encode matrix proteins with chitin binding and deacetylation
874   domains that limit tracheal tube length in Drosophila. Curr Biol 16: 186-
875   194.
876 75. Nelson KS, Khan Z, Molnar I, Mihaly J, Kaschube M, et al. (2012) Drosophila
877   Src regulates anisotropic apical surface growth to control epithelial tube
878   size. Nat Cell Biol 14: 518-525.
879 76. Wang S, Jayaram SA, Hemphala J, Senti KA, Tsarouhas V, et al. (2006) Septate-
880   junction-dependent luminal deposition of chitin deacetylases restricts
881   tube elongation in the Drosophila trachea. Curr Biol 16: 180-185.
882 77. Ochoa-Espinosa A, Baer MM, Affolter M (2012) Tubulogenesis: Src42A goes
883   to great lengths in tube elongation. Curr Biol 22: R446-449.
884 78. Olivares-Castineira I, Llimargas M (2018) Anisotropic Crb accumulation,
885   modulated by Src42A, orients epithelial tube growth in Drosophila.
886   biorxiv 287854.
887 79. Olivares-Castineira I, Llimargas M (2017) EGFR controls Drosophila tracheal
888   tube elongation by intracellular trafficking regulation. PLoS Genet 13:
889   e1006882.
890 80. Wang S, Bellen HJ (2015) The retromer complex in development and disease.
891   Development 142: 2392-2396.

892   81. Dunst S, Kazimiers T, von Zadow F, Jambor H, Sagner A, et al. (2015)
893   Endogenously tagged rab proteins: a resource to study membrane
894   trafficking in Drosophila. Dev Cell 33: 351-365.
895   82. Dutta D, Bloor JW, Ruiz-Gomez M, VijayRaghavan K, Kiehart DP (2002) Real-
896   time imaging of morphogenetic movements in Drosophila using Gal4-
897   UAS-driven expression of GFP fused to the actin-binding domain of
898   moesin. Genesis 34: 146-151.
899   83. Huang J, Huang L, Chen YJ, Austin E, Devor CE, et al. (2011) Differential
900   regulation of adherens junction dynamics during apical-basal
901   polarization. J Cell Sci 124: 4001-4013.
902   84. Shiga Y, Tanakamatakatsu M, Hayashi S (1996) A nuclear GFP beta-
903   galactosidase fusion protein as a marker for morphogenesis in living
904   Drosophila. Development Growth & Differentiation 38: 99-106.
905   85. Port F, Chen HM, Lee T, Bullock SL (2014) Optimized CRISPR/Cas tools for
906   efficient germline and somatic genome engineering in Drosophila. Proc
907   Natl Acad Sci U S A 111: E2967-2976.
908   86. Gratz SJ, Ukken FP, Rubinstein CD, Thiede G, Donohue LK, et al. (2014) Highly
909   specific and efficient CRISPR/Cas9-catalyzed homology-directed repair in
910   Drosophila. Genetics 196: 961-971.
911   87. Pfeiffer BD, Ngo TT, Hibbard KL, Murphy C, Jenett A, et al. (2010) Refinement
912   of tools for targeted gene expression in Drosophila. Genetics 186: 735-
913   755.
914   88. Richard M, Grawe F, Knust E (2006) DPATJ plays a role in retinal
915   morphogenesis and protects against light-dependent degeneration of
916   photoreceptor cells in the Drosophila eye. Dev Dyn 235: 895-907.
917   89. Schindelin J, Arganda-Carreras I, Frise E, Kaynig V, Longair M, et al. (2012)
918   Fiji: an open-source platform for biological-image analysis. Nat Methods
919   9: 676-682.
920   90. JayaNandanan N, Mathew R, Leptin M (2014) Guidance of subcellular
921   tubulogenesis by actin under the control of a synaptotagmin-like protein
922   and Moesin. Nat Commun 5: 3036.
923   91. Tomancak P, Beaton A, Weiszmann R, Kwan E, Shu S, et al. (2002) Systematic
924   determination of patterns of gene expression during Drosophila
925   embryogenesis. Genome Biol 3: RESEARCH0088.
926   92. Mishra M, Knust E (2013) Analysis of the Drosophila compound eye with
927   light and electron microscopy. Methods Mol Biol 935: 161-182.
928
929

Figure Legends

932 **Figure 1. Apn is a small transmembrane protein detected on the apical**

933 **membrane of the tracheal epithelium.**

934 (**A-F**) Expression of *apn* as detected by whole mount *in situ* hybridization (A-

935 C) and *fosapn$_{sfGFP}$* expression (D-F) in lateral views of stage 13, 15, 16, 17

936 embryos. *apn* RNA and protein appear first in fusion cells (FC) and later in the

937 dorsal trunk (DT), visceral branches (VB) and dorsal branches (DB). Scale

938 bar: 50µm.

939 (**G-H'''**) Apn-mCitrine (green) localizes on the apical plasma membrane

940 together with the apical markers SAS (G, G', G") and Uif (H, H', H"), as

941 revealed by z-projections of stage 17 tracheal tubes and optical cross

942 sections (G''' and H'''). Scale bars: (G-G" and H-H") 10µm, (G''') 5µm, (H''')

943 5µm. Arrows in G''' and H''' point to protein overlap.

944 (**I-I'''**) Tracheae of btl>apn-mCitrine stage 17 embryos stained with anti-Crb

945 (magenta) and anti-GFP (green). Cross section indicates the apical

946 localization of Apn as compared to subapical localization of Crb. Arrows in I'''

947 point to protein overlap. Scale bars: (I-I") 10µm, (I''') 3µm.

948 (**J**) Co-immunoprecipitation experiments from S2R⁺ cells expressing the

949 following constructs: UAS-Crb^{FL}+UAS-Apn^{FL} or UAS-Apn^{FL}+UAS-GFP or

950 UAS-Crb^{FL}+UAS-GFP. Crb is co-immunoprecipitated with Apn, but not with

951 GFP (used as negative control).

952

953 **Figure 2. Apnoia interacts with Crb.**

(A-B") Proximity ligation assay (PLA) shows a robust increase in number of interactions between Crb and Apn (spots in magenta) in fos*apn*sfGFP larval tracheae (A-A") as compared to control tracheae (*D*Ecad-GFP) (B-B"). Scale bar: 20μm.

(C) Quantification of the PLA signal produced between Crb and Apn as compared to Crb and *D*Ecad.

(D-E") Proximity ligation assay (PLA) shows increased numbers of interactions between Crb and Apn (spots in magenta) in fos*apn*sfGFP larval tracheae (D-D") when Crb and GFP antibodies were used as compared to fos*apn*sfGFP larval tracheae (E-E") when *D*Ecad and GFP antibodies were used. Scale bar: 50μm.

(F-G") Proximity ligation assay (PLA) shows a robust increase in number of interactions between Crb and Apn (spots in magenta) in fos*apn*sfGFP larval tracheae (F-F") as compared to a control apical protein *SAS*-Venus (G-G"). Scale bar: 50μm.

Figure 3. Apn is essential for tracheal tube maturation.

(**A-D**) Brightfield images showing the tracheal tubes of second instar larvae. Rigid and gas filled tracheal tube are present in wild type (WT) larvae (A), whereas absence of *apn* causes twisted and gas deficient tubes (B). *apn* down-regulation (*apn* RNAi) recapitulates *apn*[1] mutant tracheal defects (C). Tube morphology defects are rescued by one genomic copy of *apn* (fos.*apn*mCherry.NLS) (D). Anterior is to the left. Scale bar: 500μm.

(**E-G**) The 9th metamer of the dorsal trunk (yellow dotted line) of *apn*[1] mutant second instar larvae (F) is shorter than that of wild type larvae (WT) (E).

979 Expression of one genomic copy of *apn* (fos.*apn*mCherry.NLS) significantly

980 rescues the metamer elongation defects of *apn* mutant larvae (G). Anterior is

981 to the left. Scale bar: 200 µm.

982 **(H)** Quantification of the length of the 9th metamer of second instar tracheal

983 tubes of wild type (WT), *apn¹* mutants and *apn¹* mutants rescued with one

984 extra *apn* copy (fos.*apn*mCherry.NLS;*apn¹*). Measurements were pooled from 6

985 larvae.

986 (**I-J**) Chitin binding probe (CBP) allows the visualization of the tracheal tube

987 structure. Note the wrinkled and twisted tube of *apn¹* mutants (J) as compared

988 to that of wild type (WT) (I) larvae. Scale bar: 50µm.

989 (**K-L'**) Brightfield images to show dorsal trunk diameter expansion (K, L) and

990 gas filling (K', L') of the newly formed tracheal tube of wild type (WT, K, K')

991 and *apn¹* mutant (L, L') second larval instar. Yellow indicates the tracheal cells

992 that line along the newly formed lumen (green). Note the bubble filling the

993 newly formed lumen in wild type (WT, white arrow) (K'), which is absent in the

994 tube of *apn¹* mutants (L'), which fails to fill with gas. Scale bar: 50 µm.

995

996 **Figure 4. Apn is required for longitudinal elongation of tracheal cells.**

997 (**A-D**) Tracheal tubes of wild type (WT; A, C) and *apn¹* mutant (B, D) second

998 instar larvae stained with anti-*D*E-Cad. The long and short axes of the apical

999 surfaces (A, B) are indicated by red and green arrows, respectively, and the

1000 cells by yellow rectangles (C, D). Note that the number of cells occupying

1001 identical areas in the tracheal tube is higher (~ 4 cells) in *apn¹* mutants (D)

1002 than in WT (~ 1 cell) (C). Scale bars: 20 µm.

1003 (**E-H**) The median length of the long (E) axis is significantly smaller in apn^1

1004 mutant tracheal cells than in wild type (WT) cells as compared to the short

1005 axis, which is not affected (F). The median aspect ratio (long/short axis) (G)

1006 and the median apical surface area (H) are significantly smaller in apn^1

1007 mutant tracheal cells than in wild type (WT) cells. For box plot measurements,

1008 *n* values were calculated from 48 cells (WT) and 58 cells (apn^1).

1009

1010 **Figure 5. Apn-dependent tube growth correlates with defects in**

1011 **localization of Crb complex components**

1012 **(A-N)** Projections of confocal sections of tracheal dorsal trunks of second

1013 instar larvae. apn^1 mutants stained for the adherens junction proteins Arm (B),

1014 Polychaetoid (Pyd; D), *D*E-Cad (F) and for the apical protein Uif (H) do not

1015 display any significant changes compared to the respective wild type (WT)

1016 tissues (A, C, E, G). In contrast, localization of the Crb complex proteins, Crb

1017 (I, J) and Sdt (K, L), and the FERM protein, Moe (M, N) are mis-localized in

1018 apn^1 mutants. Scale bars: 20 µm.

1019 **(O-R')** Tracheae of second instar larvae stained for Crb (O-R) reveals strong

1020 reduction of Crb from the apical membrane and its accumulation in

1021 cytoplasmic vesicles in apn^1 mutants (P) and upon tracheal knockdown of *apn*

1022 (R). Staining for chitin binding probe (CBP; O'-R') reveals twisted tracheal

1023 tube in apn^1 mutants (P') and upon tracheal knockdown of *apn* (R'), though

1024 less severe. Expression of an additional copy of *apn* (fos.apn$_{mCherry.NLS}$)

1025 rescues Crb apical localization (Q) and tubular structure defects (Q'). Scale

1026 bar: 20 µm.

1027

Figure 6. Blocking endocytosis prevents internalization of apical Crb in *apn*-mutant tracheae.

(**A, B**) *apn¹* mutant tracheal tubes stained for Crb, after 2 hours incubation in 60µM dynasore (A) or in the absence of dynasore (B).

(**C, D**) Tracheal tubes hemizygous for the temperature sensitive *dynamin* allele, *shibire^{ts1}* stained for Crb, after 4 hours incubation at 34°C (C) and 25°C (D, as control). Scale bars: 20 µm.

Figure 7. Crb subcellular accumulation in *apn¹* mutant tracheal cells.
Projections of confocal sections of second instar tracheal tubes of transgenic lines expressing the respective YFP-tagged Rab protein stained for Crb (magenta) or YFP (green). (A", B", C") show magnifications of the boxed area in (A-A', B-B', C-C') respectively.

(**A**, **A'**) *apn¹* mutant tracheal tubes immunostained for Crb and Rab5-YFP. (A") Magnification shows vesicular Crb, most of which does not colocalize with the Rab5.

(**B**, **B'**) *apn¹* mutant tracheal tubes immunostained for Crb and Rab11-YFP. Magnification (B") shows vesicular Crb, most of which does not colocalize with Rab11.

(**C**, **C'**) *apn¹* mutant tracheal tubes immunostained for Crb and Rab7-YFP. Magnification (C") shows vesicular Crb colocalization with Rab7 of approx. 25 %. Scale bars: A, A', B, B', C, C': 20 µm and A", B", C": 5 µm.

Figure 8. Crb is localized in abnormally large, Vps35-positive vesicles in

apn¹ **mutant tracheal cells.**

(**A-A"**) Projections of confocal sections of second instar tracheal tubes, stained for Crb (magenta) and Vps35 (green). (A") shows a magnification of the boxed area in A and A'. A substantial number (approx. 79%) of Crb-positive vesicles are also positive for Vps35 in *apn¹* mutant tracheal cells.Scale bars: A, A': 20 μm and A": 5 μm.

(**B-D**) Quantification of the size of Vps35-positive vesicles (B), Arl8-positive vesicles (C) and Golgin245-positive vesicles in *apn¹* and wild type (WT) tracheal cells. Only Vps35-positive vesicles show a significant increase in size.

Figure 9. Downregulation of *crb* induces tracheal tube defects similar to those of *apn¹* mutant tubes.

(**A-D'**) RNAi- mediated downregulation of Crb (B, B' and D, D') results in strong depletion of Crb (B, D) and Sdt (B'), but does not affect Apn expression (D') in the dorsal trunk of second instar larvae. Projections of confocal sections of second instar tracheal tubes, stained for Crb (A-D), Sdt (green; A', B') and Apn (green; C', D'). Nuclear staining in C' and D' is due to an unspecific staining of Apn antibody. Scale bars: 20 μm.

(**E-H**) Brightfield images of second instar larvae showing the tracheal tubes. Tracheal tubes are rigid and gas filled in wild type (WT) (E). Reduction of Crb using either a ubiquitous (F) or a tracheal-specific (G) Gal4 recapitulates the

1074 characteristic *apn¹* mutant tracheal defects (compare F, G and H), with

1075 constricted and gas-deficient tubes. Scale bars: 20 µm.

1076 (**I-J"**) RNAi-mediated downregulation of *crb* strongly reduces Crb (compare I'

1077 and J'), but does not affect the localization of Arm or *D*E-Cad (compare I' with

1078 J' and I" with J", respectively). Scale bars: 20 µm.

1079 (**K**) Quantification of the median apical surface area of *crb* RNAi tracheal

1080 cells. The surface area is significantly reduced compared to that of wild type

1081 (WT) tracheae.

1082

1083 **Figure 10. RNAi-mediated knockdown of *crb* reduces the size of Vps35-**

1084 **positive vesicles in *apn¹* mutant tracheal cells**

1085 (**A-C**) Projections of confocal sections of second instar tracheal tubes,

1086 stained for Vps35 (green). Scale bars: A-C: 20 µm.

1087 (**D**) Quantification of the size of Vps35-positive vesicles in tracheal crb

1088 knockdown, *apn¹* mutants and double *apn¹*/crb knockdown tracheal cells.

1089

1090 **Figure 11. Model to explain Apn-mediated larval tracheal tube growth.**

1091 (**A**) Top: In the wild type (WT) dorsal trunk, the apical membrane grows along

1092 the axial axis (indicated by red arrows) and pulls the apical extracellular matrix

1093 (aECM), until the aECM resistance (indicated by green arrows) balances the

1094 forces provoked by tube elongation [33]. Bottom: In wild type tracheal cells

1095 Crb (blue) is enriched at the apical membrane where it controls apical surface

1096 growth. Apn (green) in the apical membrane is responsible for Crb

1097 maintenance and therefore ensures tube elongation. Crb trafficking involves

1098 recycling by the retromer to either the trans-Golgi network (TGN; blue

1099 vesicles) or to the plasma membrane (red vesicles), or by Rab11, or its

1100 degradation in the lysosome.

1101 (**B**) Top: In the *apn¹* mutant dorsal trunk, the pulling forces of the apical

1102 membrane expansion are decreased due to decreased growth of the apical

1103 membrane (thin red arrows), whereas the forces mediated by the aECM are

1104 likely to remain unchanged, causing breakage of the tube. Bottom: In the

1105 absence of Apn, Crb is depleted from the apical surface due to increased

1106 endocytosis. Crb is trapped in enlarged, Vps35 (retromer)-positive vesicles. It

1107 fails to be recycled (as shown by the lack of colocalization with Rab11), but is

1108 also not degraded, pointing to a functional defect of the retromer.

1109

1110 **Supporting information**

1111

1112 **Suppl. Figure 1. Amino acid sequence alignment of the protein encoded**

1113 **by CG15887 (*apn*).**

1114 Prank software of the homologous sequences within the insect order was

1115 used. Colored bars indicate the protein domains. SP: Signal Peptide, N'-ECD:

1116 N-terminal Extracellular Domain, TM: Transmembrane domain, ICD:

1117 Intracellular Domain, C'-ECD: C-terminal Extracellular Domain.

1118

1119 **Suppl. Figure 2. Apn expression in the embryonic and larval tracheae.**

1120 (**A-D**) Immunostaining of embryonic (A-B') and larval (C, D) tracheae with

1121 anti-Apn antibody shows specific tracheal staining in wild type (WT) stage 17

embryos (A) and second instar (L2) larva (C). No Apn protein can be detected in *apn¹* mutant embryos (B) and second instar (L2) larva (D). Embryos/larvae in A', B' were additionally stained for chitin binding probe (CBP) to highlight the luminal matrix. Scale bars: 20 μm.

(**E**) Yeast-two-hybrid analysis detecting interaction between the bait (Crb) and the prey (Apn). The top plate shows growth on media lacking Tryptophan and Leucine used to verify co-transformation of plasmids as well as a growth control. The bottom plate shows the same dilutions spotted on medium lacking additionally Histidine and is used to confirm the interaction between bait and prey. Column 1 is the positive control whereas columns 2,3,4 represent the negative controls (2: pB102/pP55 empty vectors, 3: pB102 empty vector/CG15887, 4: Crb/pP55 empty vector), column 5 represents the interaction between Crb-Apn. For each interaction several dilutions (undiluted, 10^{-1}, 10^{-2}, 10^{-3}) were spotted. Interactions were tested with two independent clones (A and B).

(**F**) Western blot from lysates of larval tracheae showing the expression levels of Crb and Apn in wild type (WT) and *apn¹* mutants. Tubulin is used as loading control. The 15 kDa, Apn-positive band is absent in the *apn¹* mutant extract. The higher molecular weight bands are unspecific.

(**G, G'**) Proximity ligation assay (PLA) between WT and *apn¹* mutant larval tracheae using Apn and Crb antibodies shows that the interaction is abolished in mutants lacking *apn* as compared to wild type. Scale bar: 20μm.

(**H, I**) *apn¹* mutant embryo (H) and larva (I) derived from germline clones (M/Z; maternal/zygotic).

1146 (H) No defects were observed in the tracheal tubes of mutant embryos. Scale

1147 bar: 100 μm.

1148 (I) Defects appear at second larval instar with irregular and twisted tracheal

1149 tubes (I). Scale bar: 500μm

1150 (**J**) Brightfield image of a hemizygous second instar larva transheterozygous

1151 for *apn^1* and a deficiency that removes *apn*. Scale bar: 500μm.

1152 (**K**) Body size reduction in *apn^1* mutants and tracheal knockdown larvae as

1153 compared to wild type larvae (bottom).

1154

1155 **Suppl. Figure 3. *apn* controls tube elongation independent of the aECM**

1156 **and septate junction pathway.**

1157 **(A-C)** Brightfield dorsal views of second instar larvae, showing the structure of

1158 tracheal tubes of wild type (WT) (A) and tracheal-specific *apn* down-regulation

1159 (btl>*apn* RNAi), which recapitulates *apn^1* mutant tracheal defects (B). Tube

1160 morphology defects are partially rescued by tracheal expression of Apn (*apn^1*;

1161 btl>Apn). Scale bar: 500μm.

1162 (**D-F**) The 9th metamer of the dorsal trunk (yellow dotted line) of *apn^1* mutant

1163 second instar larvae (E) is shorter than that of wild type larvae (WT) (D).

1164 Tracheal expression of a transgene (*apn^1*;btl>*apn*) rescues the metamer

1165 elongation defects of *apn* mutant larvae (F). Anterior is to the left. Scale bar:

1166 200μm.

1167 (**G-H'**) Transmission electron micrographs of cross sections through a wild

1168 type (WT; G, G') and *apn^1* mutant (H, H') second instar. (G, H) are axial views

1169 of the dorsal trunk (DT), G' and H' are higher magnifications to depict the

larval cuticular ECM (epi- and procuticle) and the taenidial ridges. Scale bars: (G,H) 7,5 μm, (G',H') 700 nm.

(**I-J'**) Immunostaining of larval tracheal tubes with antibodies against the apical extracellular matrix (aECM) proteins Dumpy (Dp) (I,J) and Piopio (I',J'). Scale bars: 20 μm.

(**K-L'**) Tracheal maturation of wild type (WT) (K, K') and apn^1 mutant (L, L') second instar larvae. Secretion of the luminal protein ANF-Cherry (E, F) as well as its clearance from the luminal space (K', L') are comparable between wild type (WT) and apn^1 mutants. Scale bars: 50 μm.

(**M-N'**) Immunostaining of wild type (WT) and apn^1 mutant tracheal tubes of second instar larvae with antibodies against the septate junction proteins Contactin (Cont) (M, N) and Discs Large (Dlg) (M', N'). Scale bar: 20 μm.

Suppl. Figure 4. Distribution of Crb in tracheal branches of distinct cellular architecture and in salivary glands.

(**A-B'''**) Confocal projections showing tracheal tubes of wild type (WT, A-A''') and apn^1 mutant (B-B''') second larval instar larvae, stained with anti-Crb. Crb localization is affected in multicellular tubes (MT), lateral branches (autocellular (AT) and seamless tubes (ST) of mutant larvae. Scale bars: (A, B, A'', B'') 20 μm and (A', B', A''', B''') 10 μm.

(**C-D'**) RNAi-mediated knockdown of *apn* by *daughterless*-Gal4 (*da*-Gal4) results in accumulation of Crb-positive cytoplasmic punctae (compare C and D) and strong reduction of Apn (compare C' and D'). Nuclear Apn signal is considered to be unspecific. Scale bars: 20 μm.

(E-F') Brightfield lateral views of second instar larvae showing the structure of multicellular tubes (MT), autocellular (AT) and seamless tubes (ST) of wild type (WT, E, E') and *apn¹* mutants (F, F'). Scale bars: (E, F) 200 µm and (E', F') 1000 µm.

(G-H') Confocal projections showing the salivary gland of wild type (WT, G, G') and *apn¹* mutants (H, H') second instar larvae, stained for Crb and Dlg. Scale bars: 20 µm.

Suppl. Figure 5. Endosomal sorting components in *apn¹* mutants.

(**A-A"**) *apn¹* mutant tracheal tubes of second instar larvae immunostained for Crb (magenta) and Hrs (green). Magnification in A" shows hardly any co-localization of vesicular Crb and Hrs.

(**B-B"**) *apn¹* mutant tracheal tubes of second instar larvae immunostained for Crb (magenta) and Lamp1 (green). Magnification in B" shows hardly any co-localization of vesicular Crb and Lamp1.

 (**C-C"**) *apn¹* mutant tracheal tubes of second instar larvae immunostained for Crb (magenta) and Arl8 (green). Magnification in C" shows hardly any co-localization of vesicular Crb and Arl8 staining. Scale bars: A, A', B, B', C, C': 20 µm and A", B", C": 5 µm.

Suppl. Figure 6. Expression of Crb of *apn¹* and *crb* depletion tracheal cells.

(A-C') RNAi-mediated downregulation of Crb (A, C) results in depletion of Crb, but does not affect Dlg expression (A', C') in the dorsal trunk of second instar larvae. In *apn¹* mutants, Crb is detected in cytoplasmic punctae (B),

1219   whereas Dlg is properly localized baso-laterally in tracheal cells (B').

1220   Projections of confocal sections of second instar tracheal tubes, stained for

1221   Crb (A-C), Dlg (green; A'-C'). Scale bars: 20 µm.

1222

Figure 1

Figure 2

Figure 3

WT — A

apn¹ — B

da>apn RNAi — C

fosapn;apn¹ — D

WT — E

apn¹ — F

fosapn;apn¹ — G

H

p=0.0145
*

p=0.00148
***

metamere legth (µm)

600
500
400
300
200
100
0

apn¹   WT   fosapn;apn¹

WT — I

apn¹ — J

WT

secretion — K

peri new lumen
old lumen

apn¹

secretion — L

new lumen
old lumen

endocytosis/ gas filling — K'

new gas
old gas

endocytosis/ gas filling — L'
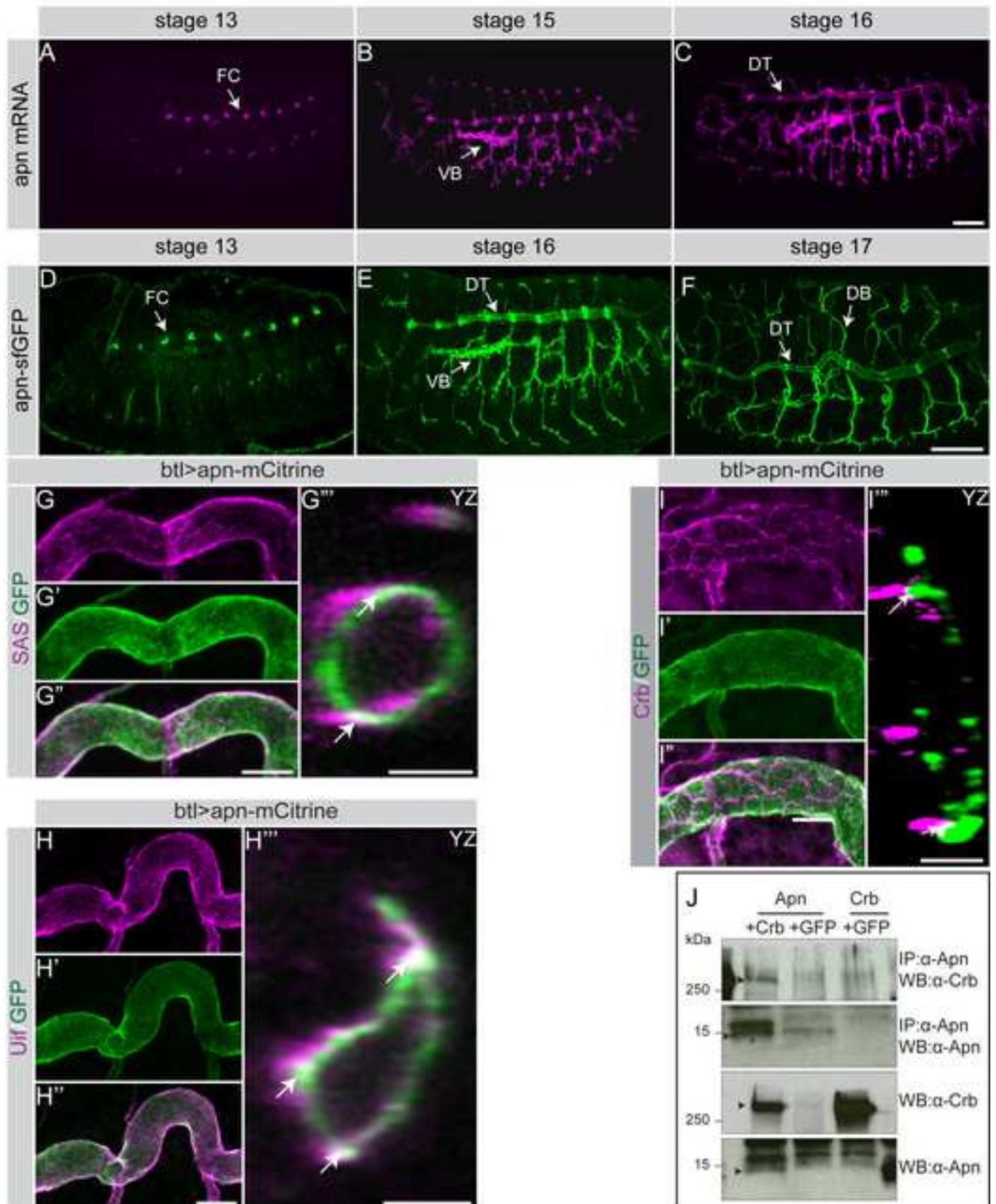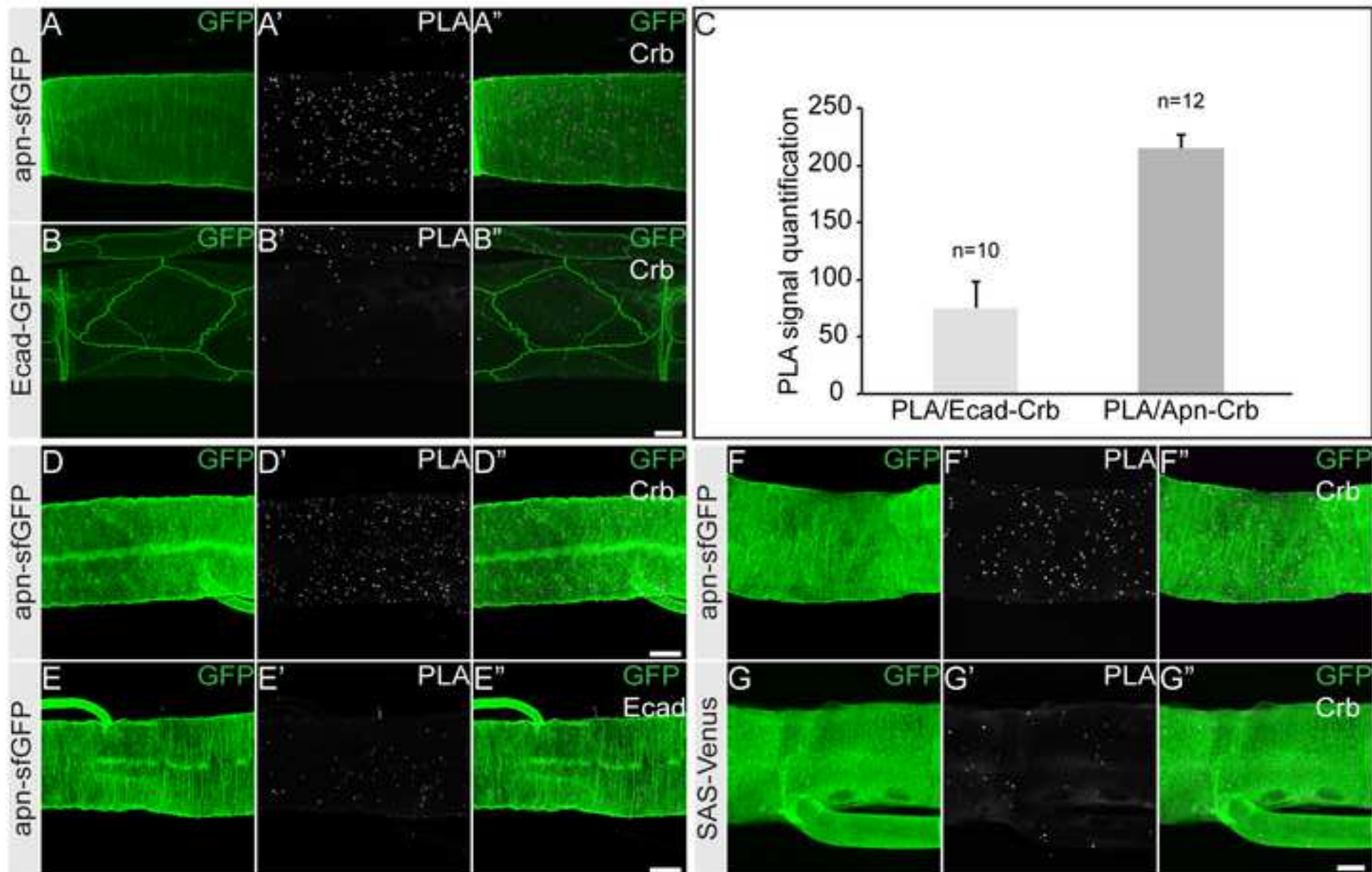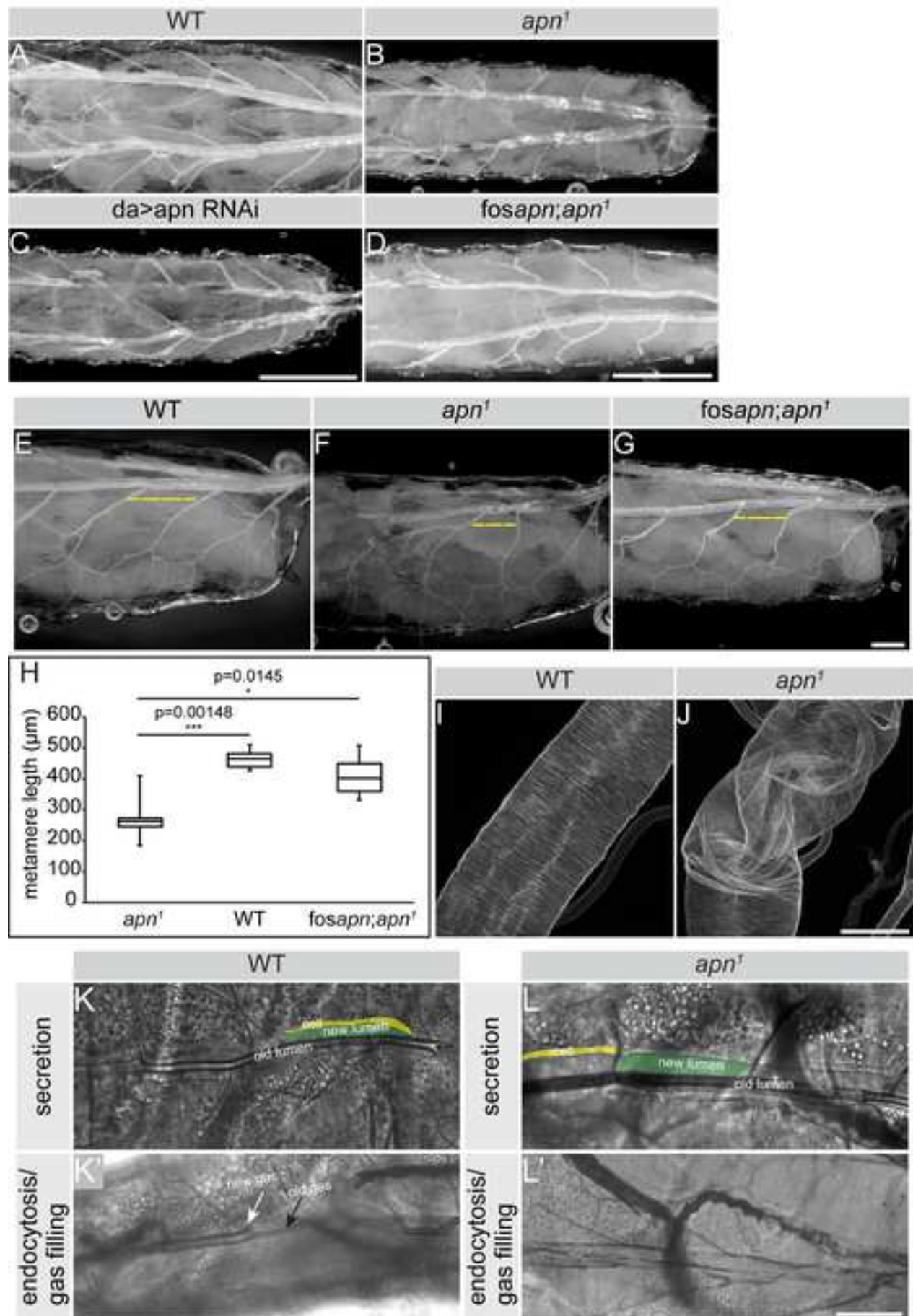
Figure 4

Figure 5

Figure 6

apn¹

| with Dynasore | w/o Dynasore |

A — Crb

B — Crb

shi^{ts1};apn¹ — 34⁰C

shi^{ts1};apn¹ — 25⁰C

C — Crb

D — Crb

Figure 7

apn¹
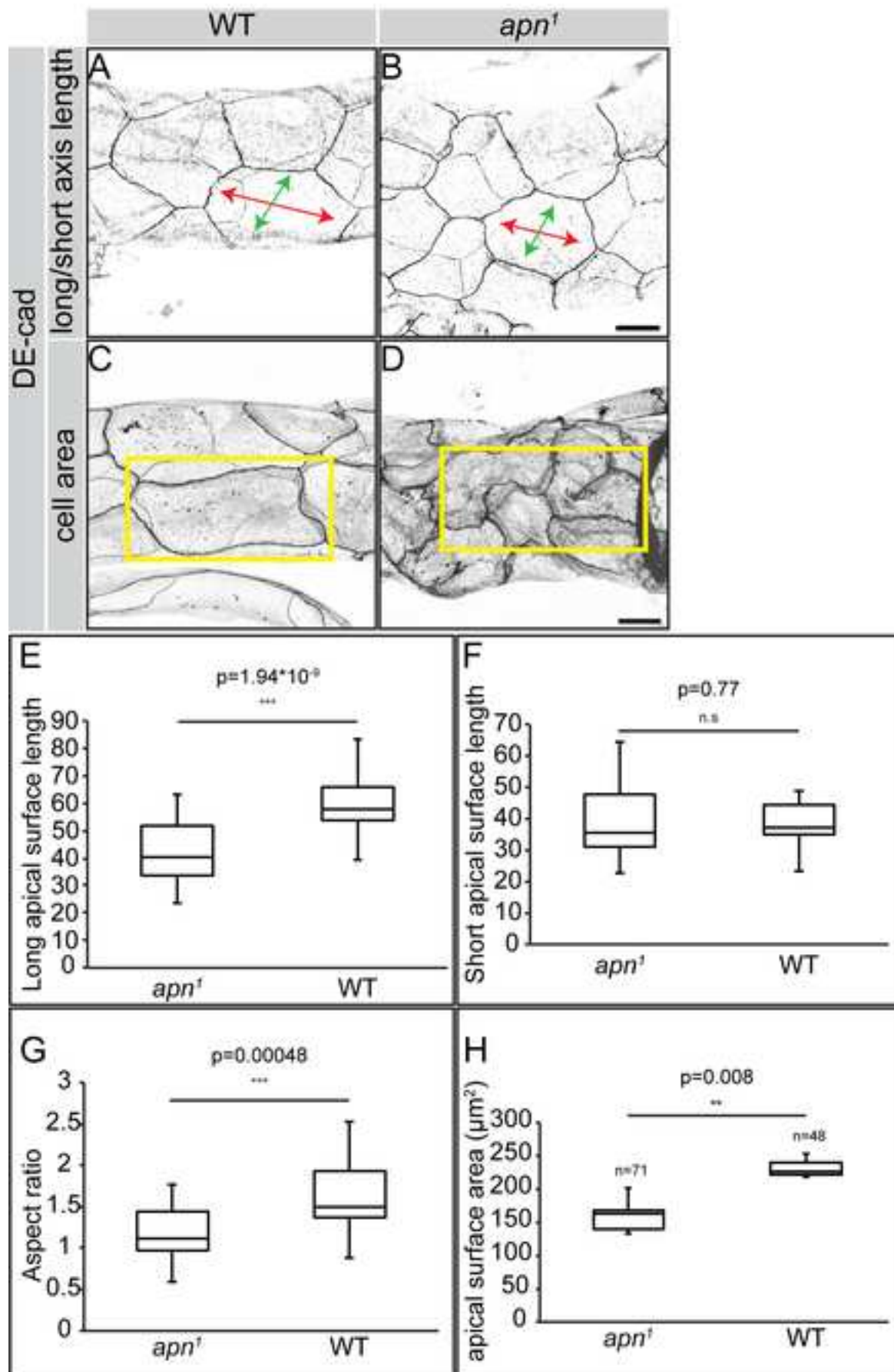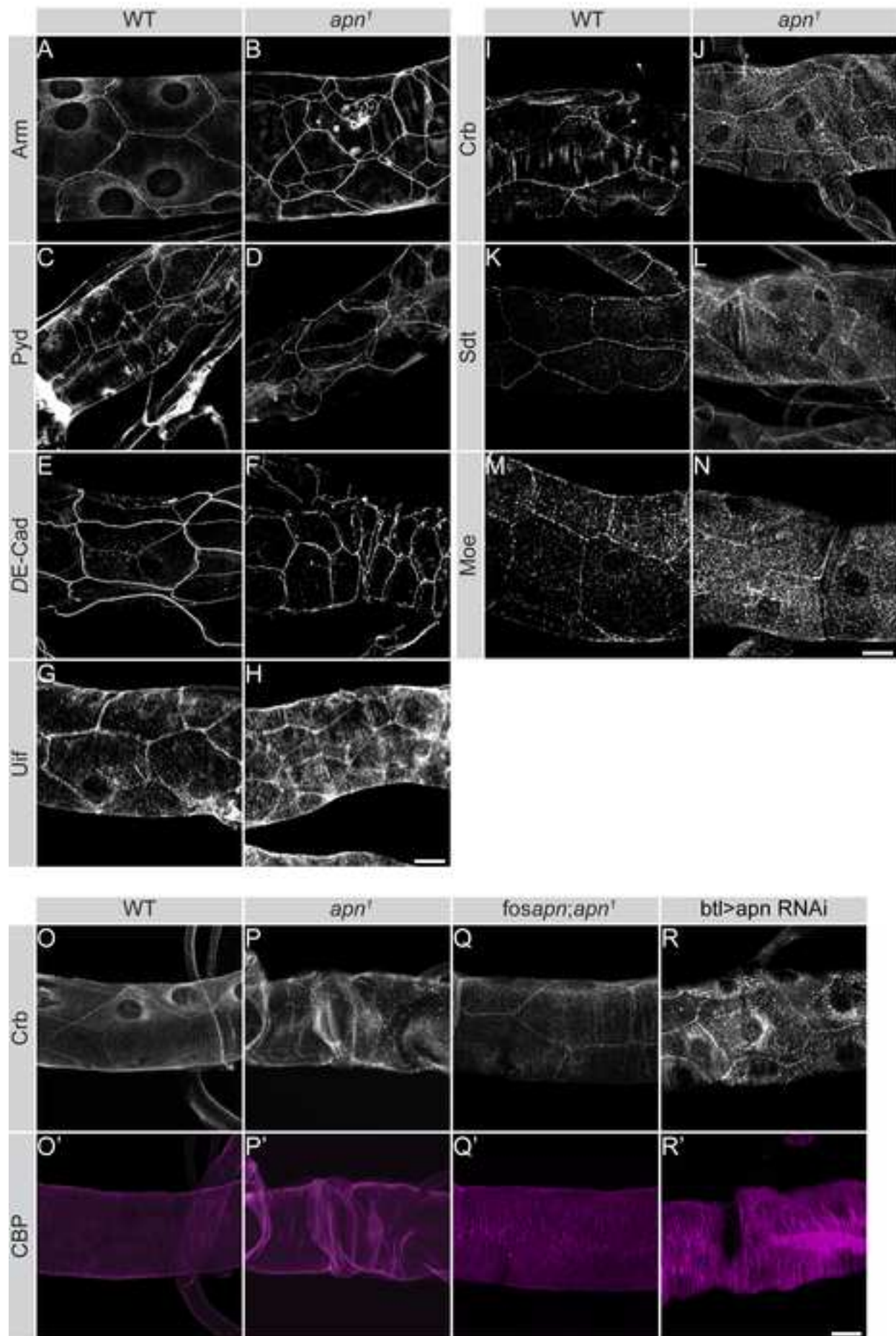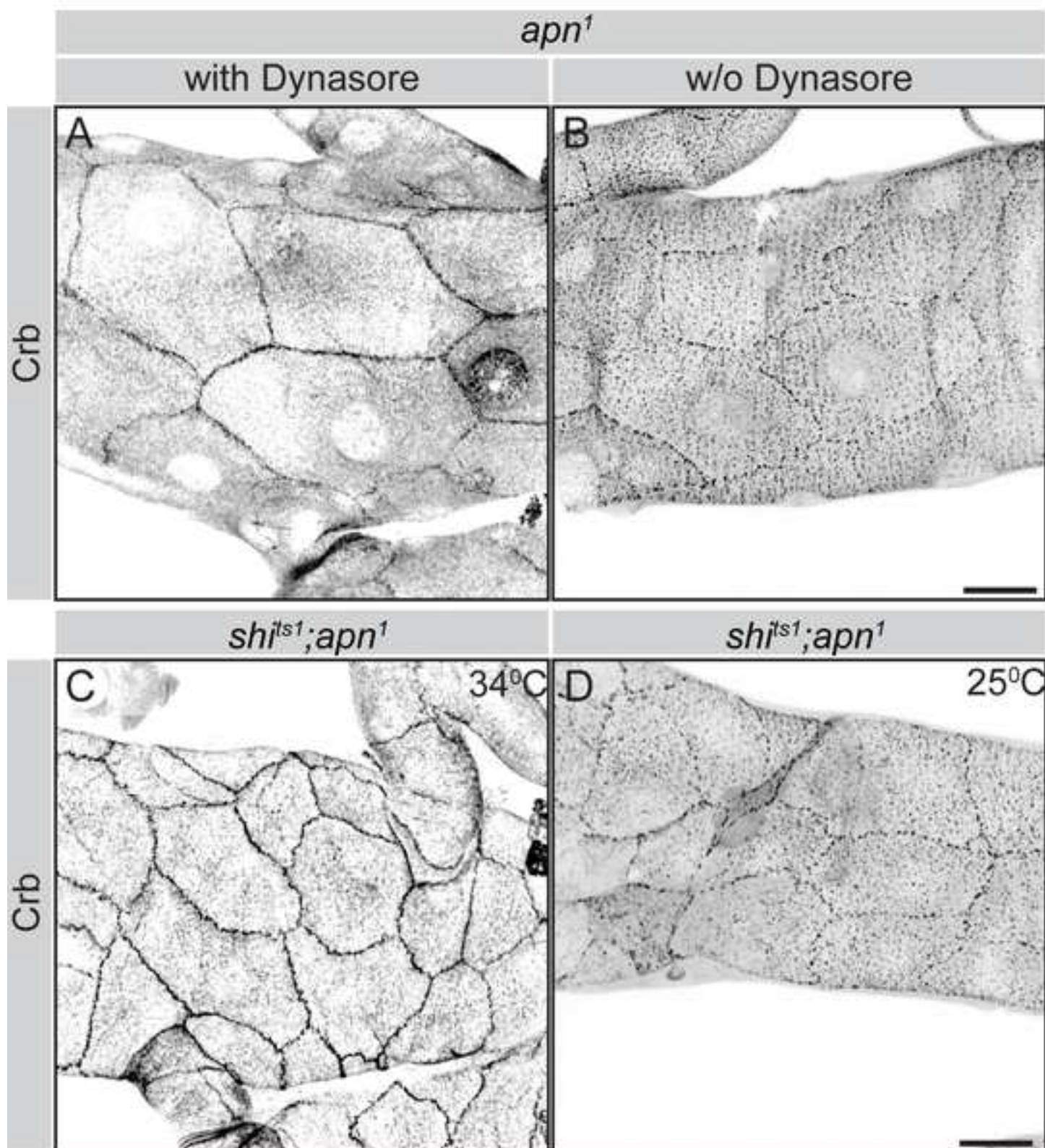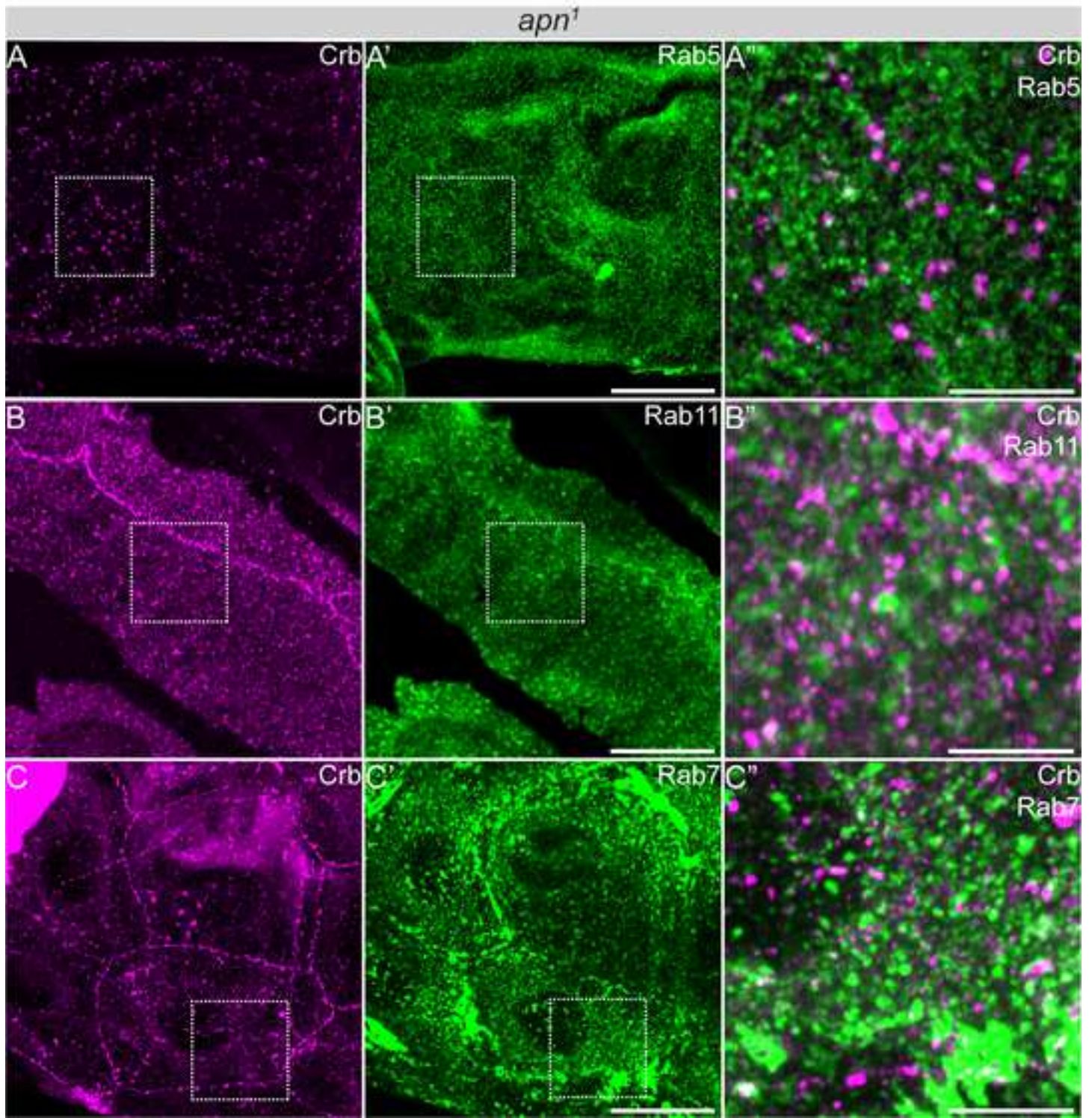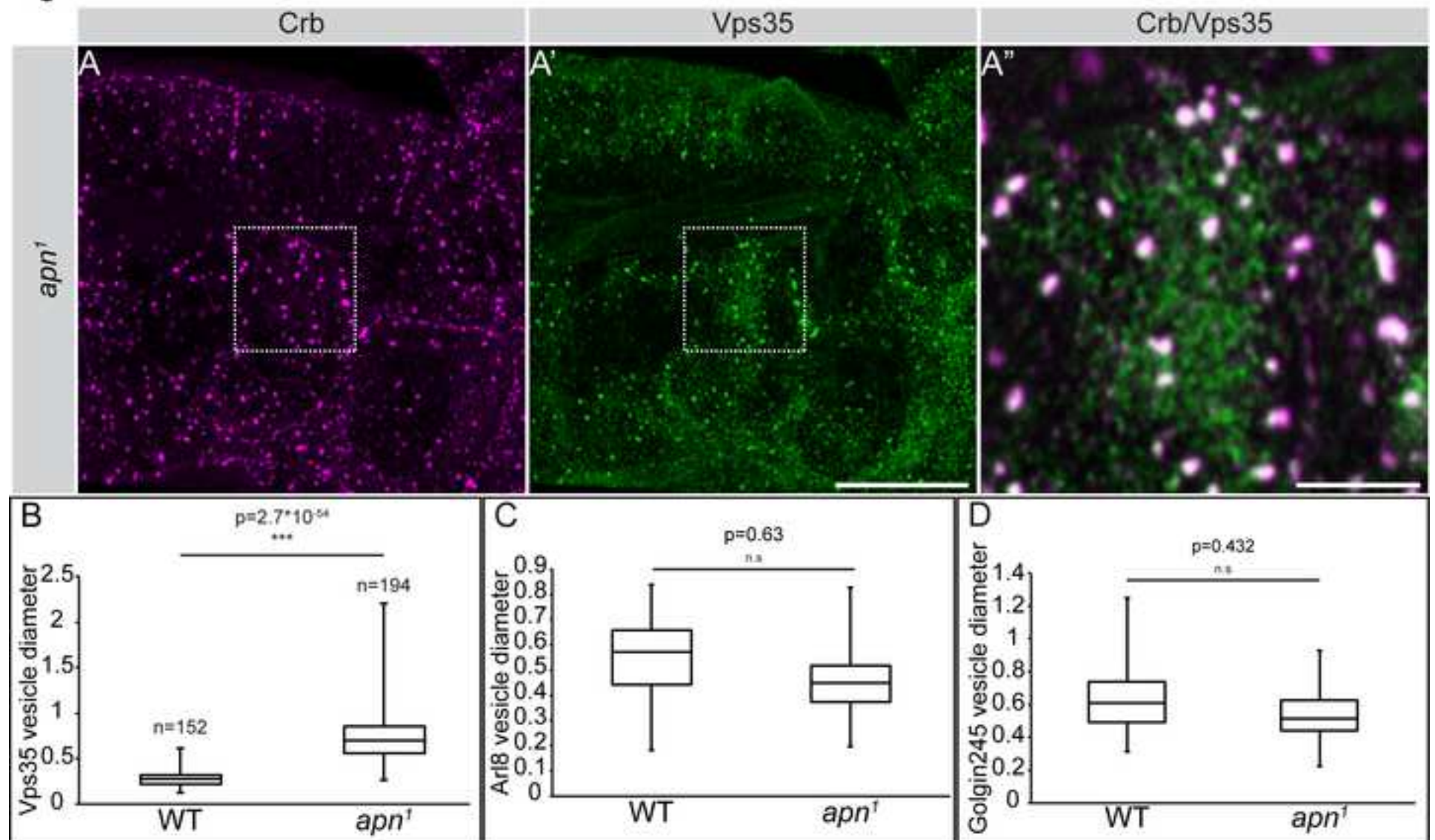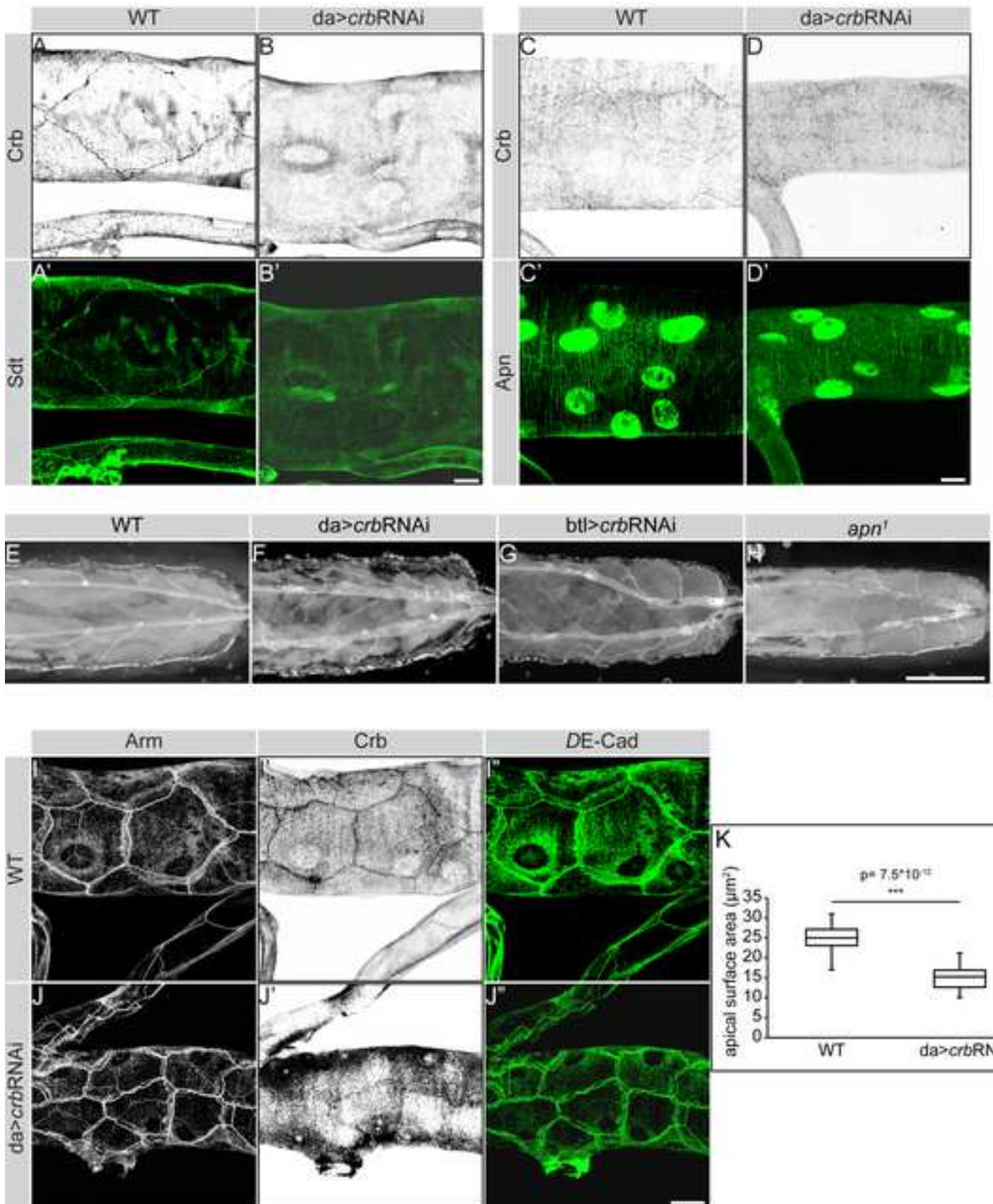
Figure 8
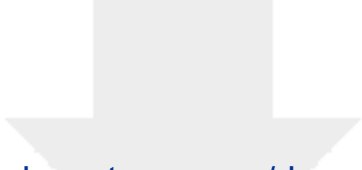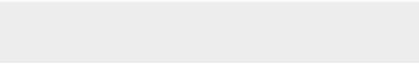
Figure 9

Figure 10
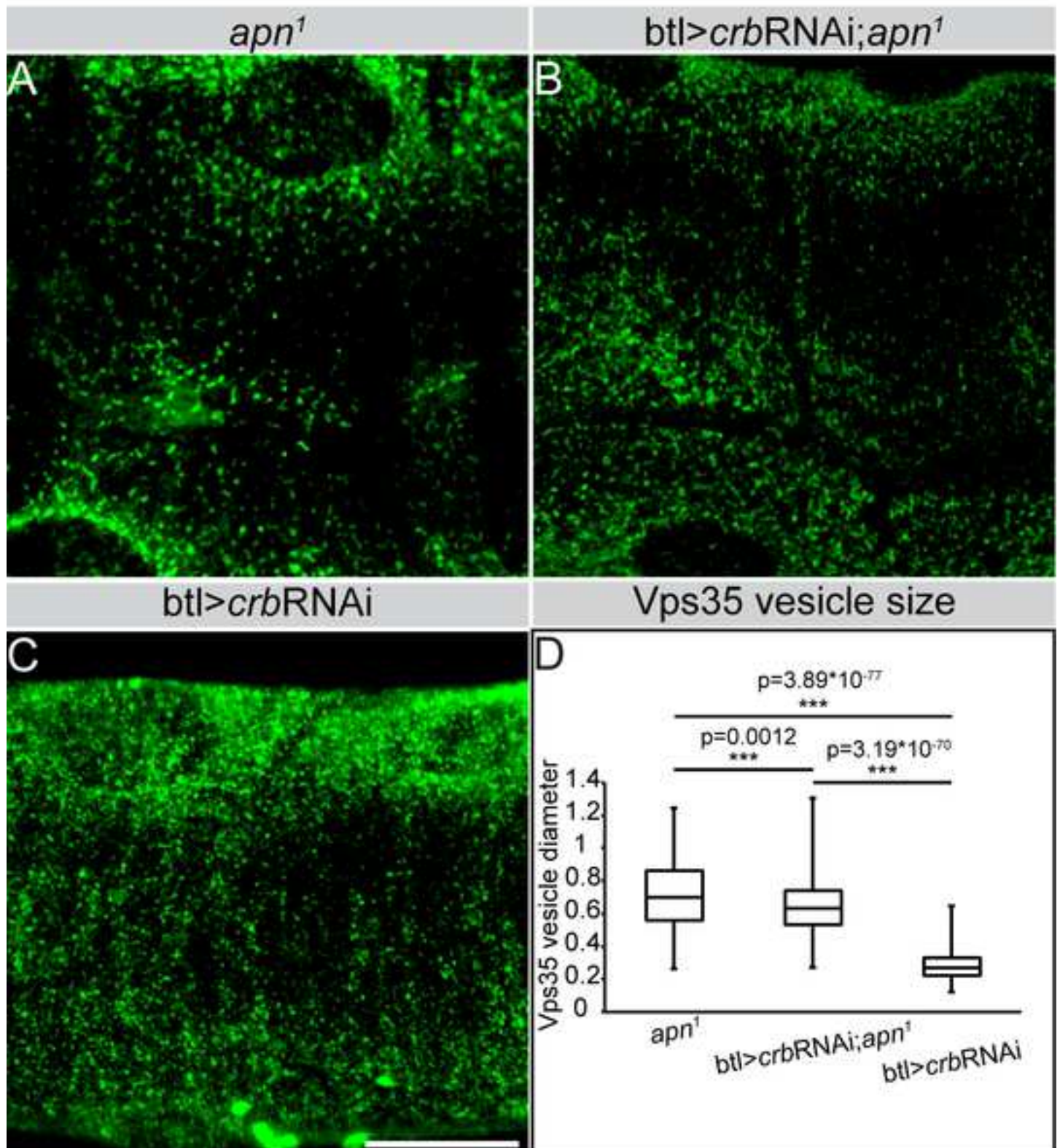
Figure 11
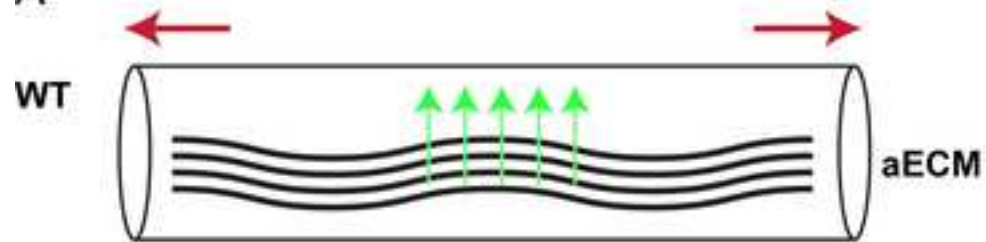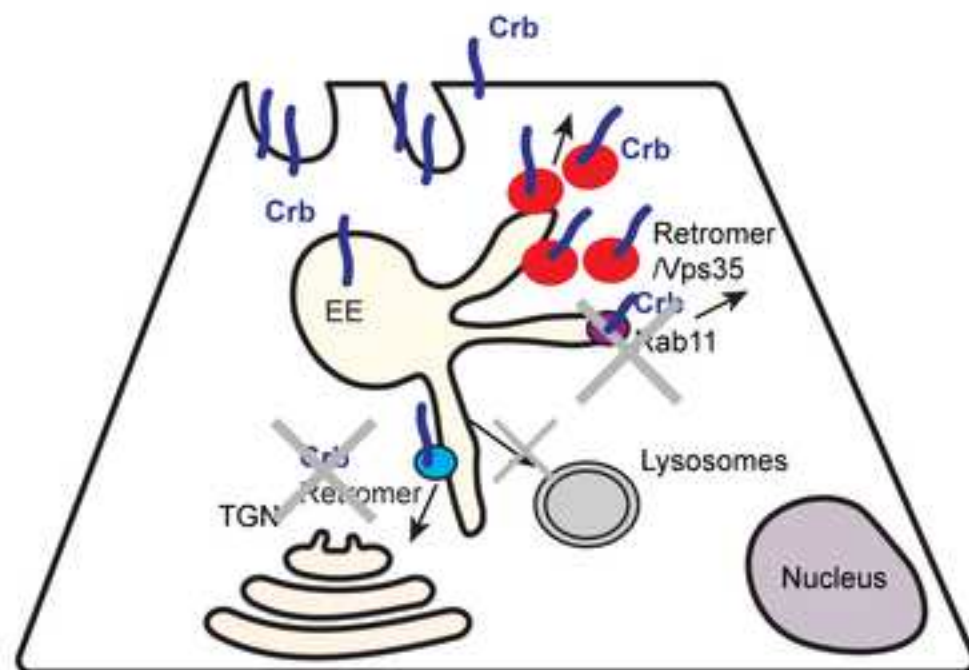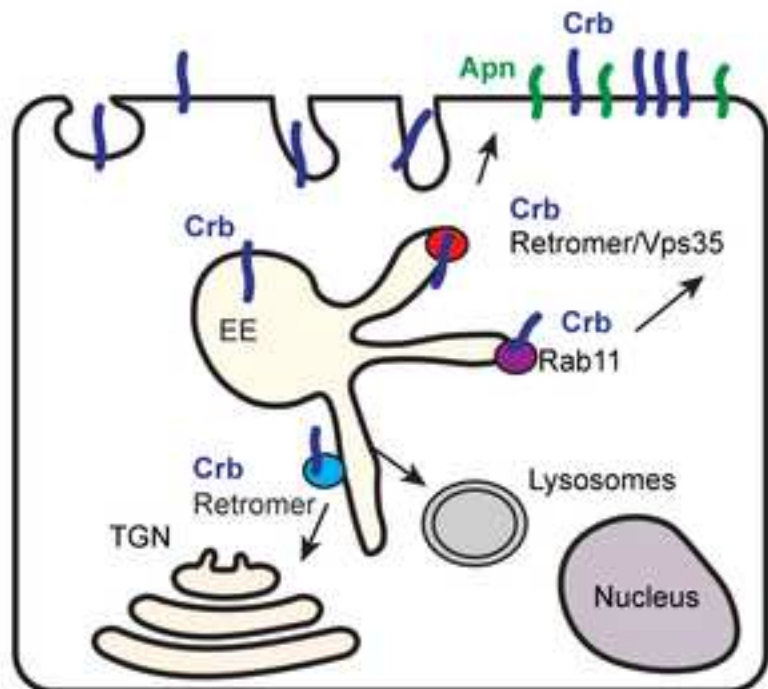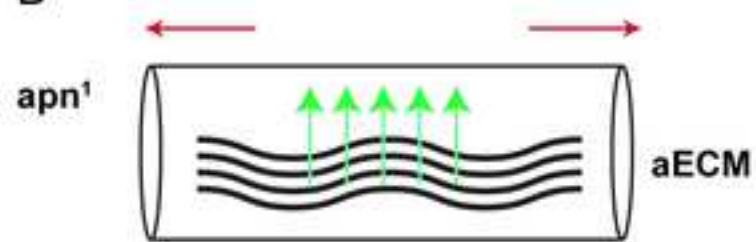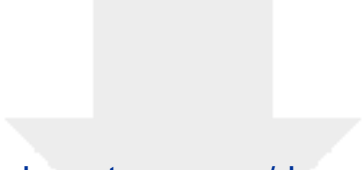
Click here to access/download
Supporting Information
Supplementary Fig1.tif

Click here to access/download
Supporting Information
Supplementary Fig2.tif

Click here to access/download
Supporting Information
Supplementary Fig3.tif

Click here to access/download
Supporting Information
Supplementary Fig4.tif

Click here to access/download
Supporting Information
Supplementary Fig5.tif

Click here to access/download
Supporting Information
Supplementary Fig6.tif

Suggested cover figure